

1N-08
380 350

TECHNICAL MEMORANDUM

X-123

EFFECT OF WING THICKNESS AND SWEEP ON THE OSCILLATING
HINGE-MOMENT AND FLUTTER CHARACTERISTICS OF A
FLAP-TYPE CONTROL AT TRANSONIC SPEEDS

By William C. Moseley, Jr., and Thomas G. Gainer

Langley Research Center
Langley Field, Va.

NATIONAL AERONAUTICS AND SPACE ADMINISTRATION
WASHINGTON

October 1959
Declassified September 1, 1961

1
2
3
4
5
6
7
8
9
10
11
12
13
14
15
16
17
18
19
20
21
22
23
24
25
26
27
28
29
30
31
32
33
34
35
36
37
38
39
40
41
42
43
44
45
46
47
48
49
50
51
52
53
54
55
56
57
58
59
60
61
62
63
64
65
66
67
68
69
70
71
72
73
74
75
76
77
78
79
80
81
82
83
84
85
86
87
88
89
90
91
92
93
94
95
96
97
98
99
100

NATIONAL AERONAUTICS AND SPACE ADMINISTRATION

TECHNICAL MEMORANDUM X-123

EFFECT OF WING THICKNESS AND SWEEP ON THE OSCILLATING
HINGE-MOMENT AND FLUTTER CHARACTERISTICS OF A
FLAP-TYPE CONTROL AT TRANSONIC SPEEDS

By William C. Moseley, Jr., and Thomas G. Gainer

SUMMARY

Free-oscillation tests were made in the Langley high-speed 7- by 10-foot tunnel to determine the effects of wing thickness and wing sweep on the hinge-moment and flutter characteristics of a trailing-edge flap-type control. The untapered semispan wings had full-span aspect ratios of 3 and NACA 65A-series airfoil sections. Unswept wings having ratios of wing thickness to chord of 0.04, 0.06, 0.08, and 0.10 were investigated. The swept wings were 6 percent thick and had sweep angles of 30° and 45° . The full-span flap-type controls had a total chord of 30 percent of the wing chord and were hinged at the 0.765-wing-chord line. Tests were made at zero angle of attack over a Mach number range from 0.60 to 1.02, control oscillation amplitudes up to about 12° , and a range of control-reduced frequencies. Static hinge-moment data were also obtained.

Results indicate that the control aerodynamic damping for the 4-percent-thick wing-control model was unstable in the Mach number range from 0.92 to 1.02 (maximum for these tests). Increasing the ratio of wing thickness to chord to 0.06, 0.08, and then to 0.10 had a stabilizing effect on the aerodynamic damping in this speed range so that the aerodynamic damping was stable for the 10-percent-thick model at all Mach numbers. The 6-percent-thick unswept-wing-control model generally had unstable aerodynamic damping in the Mach number range from 0.96 to 1.02. Increasing the wing sweep resulted in a general decrease in the stable aerodynamic damping at the lower Mach numbers and in the unstable aerodynamic damping at the higher Mach numbers. The one-degree-of-freedom control-surface flutter which occurred in the transonic Mach number range (0.92 to 1.02) for the 4-, 6-, and 8-percent-thick unswept-wing-control models could be eliminated by further increasing the ratio of thickness to chord to 0.10. Flutter could also be eliminated by increasing the wing sweep angle to either 30° or 45° . The magnitude of variation in spring moment derivative with Mach number at transonic speeds was decreased by either increasing the ratio of wing thickness to chord or increasing the wing sweep angle.

INTRODUCTION

A problem of current interest involves unstable aerodynamic damping in the control rotational mode of trailing-edge flap-type controls at transonic flight speeds. This source of aerodynamic energy can lead to a self-excited single-degree-of-freedom control flutter often called buzz. A fundamental need in dealing with this dynamic stability or aeroelastic problem is an accurate knowledge of the general factors influencing the aerodynamic moments involved in this particular oscillatory mode. Current methods for calculating unsteady aerodynamic moments do predict unstable torsional damping at low supersonic speeds for certain conditions. However, these theoretical analysis techniques are not sufficiently well developed to handle in detail either the geometric variables or the mixed flow conditions which exist for transonic flight configurations. Therefore, an experimental program was undertaken to determine some general effects of variable geometry on the aerodynamic hinge moments of this type control when oscillating about the control hinge line at transonic speeds. Some published work on this general program indicating some effects of control-hinge-line position, control profile, and control aspect ratio may be found in references 1, 2, and 3. The purpose of this paper is to present some effects of the ratio of wing thickness to chord and wing sweep on the dynamic hinge-moment and flutter characteristics of an essentially full-span trailing-edge flap-type control.

In this research program a relatively simple free-oscillation test technique is used. An unswept rectangular-wing plan form having maximum thickness-to-chord ratios of 0.04, 0.06, 0.08, and 0.10 was used in studying the effects of wing thickness. The models used to study the effects of sweep angle were untapered and had a maximum thickness-to-chord ratio of 0.06 and wing sweep angles of 30° and 45° .

Oscillating hinge moments and associated flutter characteristics were determined at an angle of attack of 0° for a range of control reduced frequency and Mach number. Control-surface oscillation amplitudes up to about 12° were investigated and some general effects of fixing boundary-layer transition by adding roughness near the wing leading edge were shown. Static hinge-moment data were also obtained.

SYMBOLS

- b twice span of semispan model, ft
- c local wing chord, ft

c_a local control chord (distance from hinge line rearward to trailing edge of control), ft

c_b local balance chord (distance from hinge line forward to leading edge of control), ft

c_t total local control chord, $c_b + c_a$, ft

C_h control hinge-moment coefficient, $\frac{\text{Hinge moment}}{2M'q}$

$$C_{h\delta} = \frac{\partial C_h}{\partial \delta}$$

$$C_{h\delta,\omega} = \frac{\text{Real part of } M_\delta}{2M'q}, \text{ per radian}$$

$$C_{h\dot{\delta},\omega} = \frac{\text{Imaginary part of } M_\delta}{2M'qk}, \text{ per radian}$$

} the subscript ω indicates an oscillatory coefficient

f frequency of control oscillation, cps

f_o control wind-off natural frequency (first mode), cps

I moment of inertia of control system about hinge line, slug-ft²

k control reduced frequency $\frac{\omega c_t}{2V}$, c_t taken at midspan of control

M effective test Mach number over span of model, $\frac{2}{\pi} \int_0^{b/2} cM_a dy$

M_a average chordwise local Mach number

M' area moment of control area rearward of and about hinge line, cu ft

M_{δ}	aerodynamic hinge moment on control per unit deflection, positive trailing edge down, ft-lb/radian
q	free-stream dynamic pressure, lb/sq ft
S	twice wing area of semispan model, sq ft
t	maximum wing thickness, ft
V	free-stream velocity, ft/sec
y	spanwise distance from plane of symmetry, ft
δ	control-surface deflection, measured in a plane perpendicular to control-surface hinge line, positive when control-surface trailing edge is below wing-chord plane, radians except as noted
δ_1	amplitude of control oscillation, deg to each side of mean control deflection
λ	logarithmic decrement, $\frac{d(\log \delta_1)}{d(\text{time})}$, per second
ω	angular frequency of oscillation, $2\pi f$, radians/sec
Λ	angle of wing sweep, deg

MODEL AND APPARATUS

The test model consisted of a semispan wing with tip store, a trailing-edge flap-type control, and a control-system spring-deflector mechanism. A schematic drawing of the test installation is shown in figure 1, and general dimensions of the models are given in figure 2. The control system was designed so that its moment of inertia about the hinge line could be varied in order to measure the dynamic hinge moments and flutter characteristics for a range of control reduced frequency.

Wing Details

The untapered, unswept wings had full-span aspect ratios of 3 and NACA 65A-series airfoil sections parallel to the free stream. Values of maximum t/c of 0.04, 0.06, 0.08, and 0.10 were investigated

(fig. 2(a)). The untapered swept wings had NACA 65A006 airfoil sections and sweep angles of 30° and 45° (fig. 2(b)).

The wings were constructed of stainless steel. Most tests were made with a tip store attached to the wing and tip stores of different weight were used to vary the wing natural frequencies. The natural first bending and torsion frequencies of the wings with the two tip stores attached are given in table I. These frequencies were obtained with the control-system spring clamped as shown in figure 1.

Control-System Details

The flap-type controls had a total chord c_t equal to 30 percent of the wing chord and were hinged at the 0.765-wing-chord line (hinge line located at 21.7 percent of the total control chord). The controls had a $0.277c_a$ blunt overhang nose balance and the gap between the control and the wing was unsealed. The control extended in the model spanwise direction from the $0.5b/2$ wing station (measured from the reflection plane) to the $0.946b/2$ wing station. The controls had a steel spar and a spruce afterportion. In order to dynamically mass balance the controls, tungsten inserts were distributed in the nose overhang and the entire control was then covered with silk.

A tang on the inboard end of the control extended through the reflection plane to the outside of the tunnel (fig. 1). The tang extension consisted of a relatively stiff rod and a torsion spring which was a short length of square rod. The control was mounted by two ball bearings outside the tunnel and a plain bearing at the wing tip. System alignment was carefully checked to keep friction to a minimum. Attached to the rod were a control position pickup and a deflector lever used to apply a step deflection to the control system. The natural frequency of the control system was varied by clamping weights of different size and inertia to the rod. The wind-off natural frequency and moments of inertia of the control system for the models tested are given in table II.

Strain gages were located near the root of the wing to indicate the wing bending and torsion responses. Control position was measured by a reluctance-type pickup located near the inboard end of the control. (See sketch in fig. 1.) Outputs of these three quantities were recorded against time by a recording oscillograph. Dynamic calibration of the recording system indicated accurate response to a frequency of about 500 cycles per second.

TESTS

The tests were made in the Langley high-speed 7- by 10-foot tunnel utilizing the side-wall reflection-plane test technique. This technique involves mounting a relatively small model on a reflection plate spaced out from the tunnel wall to bypass the tunnel boundary layer. Local velocities over the surface of the test reflection plate allowed testing to a Mach number of 1.02 without choking the tunnel. The tunnel stagnation pressure was essentially equal to sea-level atmospheric pressure.

The variation of Reynolds number based on the wing mean aerodynamic chord with test Mach number is presented in figure 3. The width of the band in figure 3 represents the maximum variation of Reynolds number with atmospheric conditions.

Oscillating hinge moments were obtained for the controls through a Mach number range of 0.60 to 1.02 for oscillation amplitudes up to about 12° . The range of control reduced frequency k varied with Mach number and control-system inertia and was generally in the range from 0.04 to 0.16. In addition, static hinge moments were obtained for all controls. All tests were made at a wing angle of attack of 0° .

A majority of the tests were made with roughness added to the wing surface to insure boundary-layer transition from laminar to turbulent flow conditions. A single layer of No. 240 carborundum grains, $\frac{1}{16}$ -inch wide was applied to both surfaces of the wing at the 0.05-chord line. However, a few tests were run "transition free," that is, with no carborundum grains applied to the wing as a check on the effects of adding roughness for these tests.

TEST TECHNIQUE AND REDUCTION OF DATA

The model was designed so that a free-oscillation test technique could be used. At the control rotational frequencies tested, the response of the control surface was essentially a single-degree-of-freedom rotation about the hinge line. Care was taken to keep to a minimum the wing vibration response to the control forcing function. Inertia coupling between the wing and control was eliminated by dynamically mass balancing the control about the hinge line and the response of the wing to the aerodynamic forcing function resulting from deflection of the control could be influenced to some degree by proper choice of the tip-store weight. Since the physical response of the model for the various test conditions was predominantly control rotation, the aerodynamic moment resulting

from angular deflection of the control about the hinge line could be determined from the free-oscillation characteristics of the control system subsequent to known starting condition. Representative oscillograph records of the time response of the model are shown in figure 4.

The technique used to initiate the free oscillations depended on the total damping (aerodynamic plus nonaerodynamic) of the control system for the particular test condition. When the total damping was unstable at low deflections, the hinge moments were determined from the unstable oscillation following release of the control at $\delta \approx 0^\circ$ (fig. 4(c)). This type of oscillation was initiated by random tunnel disturbances and, in all cases tested, was self-limiting in amplitude. When the total damping was stable or varied from stable to unstable within the test oscillation-amplitude range, the free oscillation was initiated by releasing the control at some deflection angle (figs. 4(a) and (b)). The mean oscillation amplitude for this investigation was very near 0° deflection in all cases.

Evaluation of Spring Moments

The aerodynamic inphase or spring moment was determined from the natural frequency of oscillation of the control system. Since the variation of inphase moment with amplitude is not necessarily linear and the test method was not sufficiently accurate to determine the variation in natural frequency with amplitude, the values of $C_{h\delta,\omega}$ presented are effective values averaged over some amplitude range of the oscillation. In this investigation, the effect of the values of damping on the natural frequency was considered negligible, and the aerodynamic spring-moment derivative was determined from the relationship

$$C_{h\delta,\omega} = \frac{I(\omega_0^2 - \omega^2)}{2M'q} \quad (1)$$

where the subscript o signifies a wind-off condition. As shown by equation (1), negative values of $C_{h\delta,\omega}$ oppose the control displacement and hence increase the stiffness or natural frequency of the control surface.

Evaluation of Damping Moments

The aerodynamic out-of-phase or damping moment was determined from the rate of buildup or decay of the free oscillation of the control system. The damping moment is not necessarily linear with amplitude;

however, the damping moments were analyzed on the basis of an equivalent linear system. It was assumed that the damping forces were adequately described by an equivalent viscous damping and that the time response of the actual system was simulated by a linear system having the appropriate damping constant at each oscillation amplitude for a given frequency. The variation of damping-moment derivative with oscillation amplitude was obtained by plotting the logarithm of the amplitude of successive cycles of the oscillation against time and taking the slope at any given amplitude of the paired curves as the value of the logarithmic decrement $\lambda = \frac{d(\log \delta_1)}{d(\text{time})}$ of the oscillation. The aerodynamic damping derivative was determined from the relationship

$$C_{h\dot{\delta},\omega} = \frac{4.6IV}{qM'c_t}(\lambda - \lambda_0) \quad (2)$$

where the subscript 0 refers to the wind-off values taken at approximately the same frequency and amplitude as the wind-on values.

The aerodynamic damping derivative is related to an equivalent viscous damping constant C in $\frac{\text{ft-lb}}{\text{radians/sec}}$ by the expression

$$C = C_{h\dot{\delta},\omega} \frac{c_t q M'}{V} \quad (3)$$

Determination of Static Hinge Moments

Static hinge moments were measured by restraining the control system in torsion with a calibrated electric strain-gage beam which measured the torque or moment about the control hinge line for various control deflections. The static hinge-moment coefficient C_h was determined from the relationship

$$C_h = \frac{\text{Hinge moment}}{2M'q} \quad (4)$$

Corrections

No corrections have been applied to the data for the chordwise and spanwise velocity gradients or for the effects of the tunnel walls. It is shown in reference 4 that a tunnel resonance phenomenon can appreciably decrease the magnitude of forces and moments measured in oscillation tests. However, it is believed that this phenomenon had no appreciable effect on the results of the present investigation. In general, most of the test frequencies were well removed from the calculated resonant frequencies, and there was no apparent decrease in moments for the test frequencies that were close to resonant frequencies. It is possible that the magnitude of the resonant effects would be relieved by the model tip effects and the nonuniformity of the velocity field in the test section.

Static control-deflection corrections have been applied to the output of the position pickup to give the deflection at the midspan of the control surface for the static tests. No deflection corrections have been applied to the oscillatory data to account for any twist of the control system outboard of the position pickup (fig. 1(a)) since, for the physical constants and frequencies involved, a brief analysis and analog studies have indicated that this was a secondary effect.

RESULTS AND DISCUSSION

Damping Moments and Flutter Characteristics

The variation of aerodynamic damping coefficient $C_{h\delta, \omega}$ with oscillation amplitude for various Mach numbers and reduced frequencies together with the associated flutter characteristics are presented in figure 5 for the various ratios of wing thickness to chord investigated and in figure 6 for the two swept wings investigated. Shown in figures 7 and 8, respectively, are cross plots of the data from figures 5 and 6 to show the effects of wing thickness and wing sweep on the variation of $C_{h\delta, \omega}$ with Mach number at arbitrarily selected amplitudes and reduced frequencies.

The data of figures 5 and 6 show a nonlinear variation of damping coefficient $C_{h\delta, \omega}$ with oscillation amplitude, particularly at Mach numbers above $M = 0.90$. Values of reduced frequency k for each Mach number are given in the tables on figures 5 and 6 since for the type of test technique used it was not feasible to maintain a constant reduced frequency throughout the Mach number range investigated. Also given are

flutter amplitudes and frequencies for all conditions where flutter occurred. Some scatter or erratic variations in $C_{h\delta,\omega}$ can be expected as a normal occurrence for this type of test technique; however, the general trends are considered valid. Although care was taken to check the alinement of the control system, some difficulties were encountered in keeping the tare or friction damping constant and small in the bearing system that was made necessary by the relatively large control oscillation amplitudes studied in these tests. Tare or wind-off damping values were determined before and after each test, and average values were used for the test.

Most of the tests were made with a roughness strip near the wing leading edge. It was expected that in most full-scale conditions the boundary layer would be turbulent. Since the boundary layer can have important effects on the pressure distribution on flap-type controls it was considered desirable to have a turbulent boundary layer for these tests in an effort to keep results consistent with full-scale conditions. No boundary-layer surveys were made to determine if there were any basic changes in the boundary layer for the tests with roughness removed (transition free). Some differences are noted particularly for figure 5(d); however, no major trend effects are apparent which can be attributed to the effects of fixing transition for these test results. Tests were made with the tip store removed on the wing-control model with $t/c = 0.04$ (fig. 5(a)) and the results indicate very little effect on the variation of the aerodynamic damping moment.

The data for the wing-control model with $t/c = 0.04$ (fig. 5(a)) indicate that at the lower Mach numbers $M = 0.60$ to $M = 0.90$ the aerodynamic damping was stable throughout the amplitude and reduced-frequency range investigated. In general, the damping coefficient $C_{h\delta,\omega}$ was fairly constant through the amplitude range with only small variations with reduced frequency occurring. As the Mach number was increased above $M = 0.90$ an unstable shift in aerodynamic damping generally occurred, resulting in unstable values of aerodynamic damping in the Mach number range from 0.92 to 1.02. Maximum unstable values of $C_{h\delta,\omega}$ generally occurred at the lower oscillation amplitudes with unstable values of $C_{h\delta,\omega}$ decreasing with increase in oscillation amplitude, thus leading to the limited-amplitude-type flutter response obtained. Increasing t/c for the wing-control model generally resulted in a stabilizing effect at the higher test Mach numbers (0.92 to 1.02). A cross plot of the data of figure 5 at two arbitrarily chosen amplitudes and reduced frequencies further illustrates the effect of thickness on this unstable shift in aerodynamic damping in the transonic Mach number range. (See fig. 7.)

Tests were made with the tip store removed on the wing-control model with $t/c = 0.04$ (fig. 5(a)) and the results indicate very little effect on the variation of the aerodynamic damping moment.

When comparing the flutter characteristics (fig. 5) with the aerodynamic damping values it should be remembered that the control system had a certain level of tare or nonaerodynamic damping. Flutter was a self-excited oscillation involving only the degree of freedom of control rotation about the hinge line. In some cases flutter was self-starting and built up until a steady-state condition was reached, whereas in other cases it was necessary to deflect the control before flutter occurred. The flutter frequencies and amplitudes given are for the constant-amplitude oscillatory conditions wherein the energy fed into the oscillation over a complete cycle was equal to the energy dissipated by nonaerodynamic damping present in the system. The effect of increasing maximum ratio of wing thickness to chord was a reduction in the Mach number range over which flutter occurred. For the wing-control model with $t/c = 0.04$, flutter occurred over the Mach number range from $M = 0.94$ to $M = 1.02$, whereas for the wing-control model with $t/c = 0.10$ no flutter occurred over the Mach number range investigated. It might be well to note here that flutter has been obtained on models with thick sections (for example, ref. 5). However, many differences in configuration existed such as wing taper and camber, control overhang balance, and hinge line.

The 30° and 45° swept wings had maximum thickness-to-chord ratios of 0.06 and for comparison purposes the damping data of the unswept wing with $t/c = 0.06$ will be briefly reemphasized here. The aerodynamic damping for the unswept wing was stable for all amplitudes and reduced frequencies for the lower Mach numbers investigated (0.60 to 0.90). In general, $C_{h\delta, \omega}$ was fairly constant with amplitude for this Mach number range with only small erratic variations with reduced frequency. As Mach number was increased above $M = 0.90$ an unstable shift in aerodynamic damping generally occurred for the unswept wing resulting in unstable aerodynamic damping above $M = 0.94$, and some flutter was encountered as noted in the table in figure 5(b). The larger values of unstable damping occurred at the lower amplitudes investigated. Increasing the wing sweep to 30° and to 45° had a small destabilizing effect on $C_{h\delta, \omega}$ at the lower Mach numbers but resulted in a stabilizing effect in the Mach number range from $M = 0.96$ to $M = 1.02$. These effects are more clearly shown in figure 8 for arbitrarily chosen values of reduced frequency and oscillation amplitude. Although at the higher reduced frequencies investigated, small unstable values of aerodynamic damping were still present for the 30° swept-wing-control model (fig. 8(a)) sufficient nonaerodynamic damping was present in the model control system to prevent flutter. Variation in reduced frequency had

only small effects on the aerodynamic damping. The effects of adding surface roughness to insure a turbulent boundary layer were small with no systematic variation with Mach number or oscillation amplitude being noted.

Spring Moments

Static hinge-moment or spring-moment coefficients are shown in figures 9 and 10 for the wing-control models investigated. The variation of static and dynamic spring-moment derivatives $C_{h\delta}$ and $C_{h\delta,\omega}$ with Mach number is shown in figure 11. At the lower Mach numbers (0.60 to 0.90) the variation of C_h with control deflection for the wing-control model with $t/c = 0.04$ was generally underbalanced and linear at the lower deflections ($\delta = \pm 5^\circ$) and became more underbalanced at the higher deflections. In the Mach number range from 0.95 to 1.02 (maximum for these tests), the variation of C_h with δ became more underbalanced as the aerodynamic-loading center shifted rearward until, at $M = 1.02$, C_h was generally linear throughout the δ -range investigated. The principal effect of increasing maximum t/c was a reduction in the control underbalance particularly near $\delta = 0^\circ$. This resulted in static instability or overbalance for the wing-control model with $t/c = 0.10$ near $M = 0.95$. Previously published data (refs. 6 and 7) have indicated similar results and it is believed that the change in trailing-edge angle which accompanies the increase in thickness-to-chord ratio is the primary cause.

The variation of C_h with control deflection for the swept-wing-control models (fig. 10) shows that increasing the wing-sweep angle results in a reduction of control underbalance throughout the Mach number range investigated.

The variation of spring-moment derivatives with Mach number from both static ($C_{h\delta}$) and dynamic ($C_{h\delta,\omega}$) tests is shown in figure 11 for both the unswept- and swept-wing-control models. It should be noted here that the free-oscillation test technique used in these tests is not particularly good for determining inphase moments because of the difficulty of accurately determining the oscillation frequency over a limited number of cycles. It was not possible to determine the variation of oscillation frequency with amplitude and in some cases the dynamic derivatives were necessarily evaluated over an amplitude range where the static hinge-moment data were nonlinear with amplitude. The static derivative $C_{h\delta}$ was generally measured over a δ -range of $\pm 5^\circ$ and when possible the dynamic data $C_{h\delta,\omega}$ were also measured over a similar oscillation amplitude range.

CONCLUSIONS

Results of tests at Mach numbers from 0.60 to 1.02 to determine the effect of wing thickness and sweep on the oscillating hinge-moment and flutter characteristics of a flap-type control indicate the following conclusions:

1. The control aerodynamic damping for the 4-percent-thick wing-control model was unstable in the Mach number range from 0.92 to 1.02 (maximum for these tests). Increasing the thickness-to-chord ratio to 0.06, 0.08, and then to 0.10 had a generally progressive stabilizing effect on the aerodynamic damping so that the aerodynamic damping was stable for the thickness-to-chord ratio of 0.10 model except at the higher test Mach numbers (1.00 and 1.02).

2. The aerodynamic damping in the control rotational mode for the 6-percent-thick unswept-wing-control model was stable at the lower Mach numbers up to about 0.94 and generally unstable at the higher Mach numbers (0.96 to 1.02). Increasing the wing sweep resulted in a general decrease in the stable aerodynamic damping at the lower Mach numbers and a decrease in the unstable aerodynamic damping at the higher Mach numbers.

3. A one-degree-of-freedom control-surface flutter occurred in the transonic Mach number range (0.92 to 1.02) for the 4-percent-thick unswept-wing-control model. This Mach number range was progressively decreased as wing thickness was increased to 6 percent and 8 percent, and flutter was completely eliminated by further increasing wing thickness to 10 percent. Flutter was also eliminated by increasing the wing-sweep angle to either 30° or 45° .

4. An increase in wing thickness or wing-sweep angle had a balancing effect on the spring-moment coefficient and decreased the magnitude of the variation of spring-moment derivative with Mach number at transonic speeds.

Langley Research Center,
National Aeronautics and Space Administration,
Langley Field, Va., July 16, 1959.

REFERENCES

1. Thompson, Robert F., and Moseley, William C., Jr.: Oscillating Hinge Moments and Flutter Characteristics of a Flap-Type Control Surface on a 4-Percent-Thick Unswept Wing With Low Aspect Ratio at Transonic Speeds. NACA RM L55K17, 1956.
2. Thompson, Robert F., and Moseley, William C., Jr.: Effect of Hinge-Line Position on the Oscillating Hinge Moments and Flutter Characteristics of a Flap-Type Control at Transonic Speeds. NACA RM L57C11, 1957.
3. Moseley, William C., Jr., and Price, George W., Jr.: Effects of Control Profile on the Oscillating Hinge-Moment and Flutter Characteristics of a Flap-Type Control at Transonic Speeds. NACA RM L57E27, 1957.
4. Runyan, Harry L., and Watkins, Charles E.: Considerations on the Effect of Wind-Tunnel Walls on Oscillating Air Forces for Two-Dimensional Subsonic Compressible Flow. NACA Rep. 1150, 1953. (Supersedes NACA TN 2552.)
5. Erickson, Albert L., and Stephenson, Jack D.: A Suggested Method of Analyzing For Transonic Flutter of Control Surfaces Based on Available Experimental Evidence. NACA RM A7F30, 1947.
6. Thompson, Robert F.: Investigation of a 42.7° Sweptback Wing Model To Determine the Effects of Trailing-Edge Thickness on the Aileron Hinge-Moment and Flutter Characteristics at Transonic Speeds. NACA RM L50J06, 1950.
7. Lowry, John G., Axelson, John A., and Johnson, Harold I.: Effects of Sweep on Controls. NACA RM L8A28c, 1948.

TABLE I

NATURAL FIRST BENDING AND TORSION FREQUENCIES OF WING

Wing with -	Tip store used	Bending, cps	Torsion, cps
t/c = 0.04	Light	125	485
	Heavy	97	318
t/c = 0.06	Light	175	(a)
	Heavy	130	700
t/c = 0.08	Light	206	(a)
	Heavy	164	(a)
t/c = 0.10	Light	250	(a)
	Heavy	200	(a)
30° of sweep	Light	135	570
	Heavy	114	470
45° of sweep	Light	81	433
	Heavy	65	350

^aTorsion mode not obtained.

TABLE II

MOMENT OF INERTIA AND WIND-OFF NATURAL FREQUENCY OF CONTROL SYSTEMS

Configuration	I, slug-ft ²	f _o , cps
t/c = 0.04 wing	1.02 × 10 ⁻⁵	331.5
t/c = 0.04 wing plus small inertia weight	2.34	218
t/c = 0.04 wing plus large inertia weight	6.57	129.5
t/c = 0.06 wing	1.07	326
t/c = 0.06 wing plus small inertia weight	2.39	216.5
t/c = 0.06 wing plus large inertia weight	6.62	129
t/c = 0.08 wing	1.07	317.5
t/c = 0.08 wing plus small inertia weight	2.39	215
t/c = 0.08 wing plus large inertia weight	6.62	129
t/c = 0.10 wing	1.08	322
t/c = 0.10 wing plus small inertia weight	2.39	216
t/c = 0.10 wing plus large inertia weight	6.63	130
30° wing	.91	299
30° wing plus small inertia weight	2.24	191
30° wing plus large inertia weight	6.46	114.2
45° wing	.88	303
45° wing plus small inertia weight	2.20	194
45° wing plus large inertia weight	6.43	116

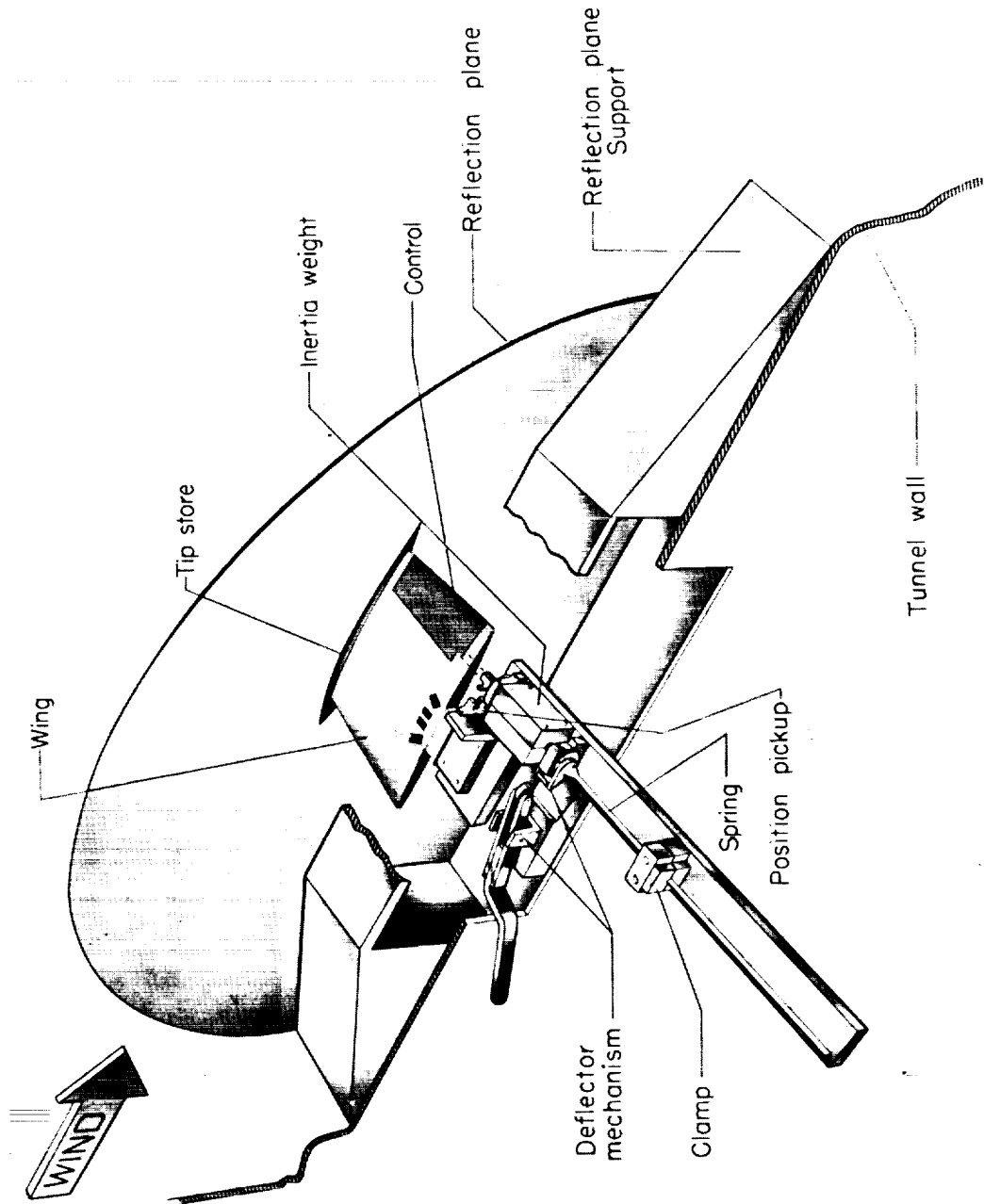
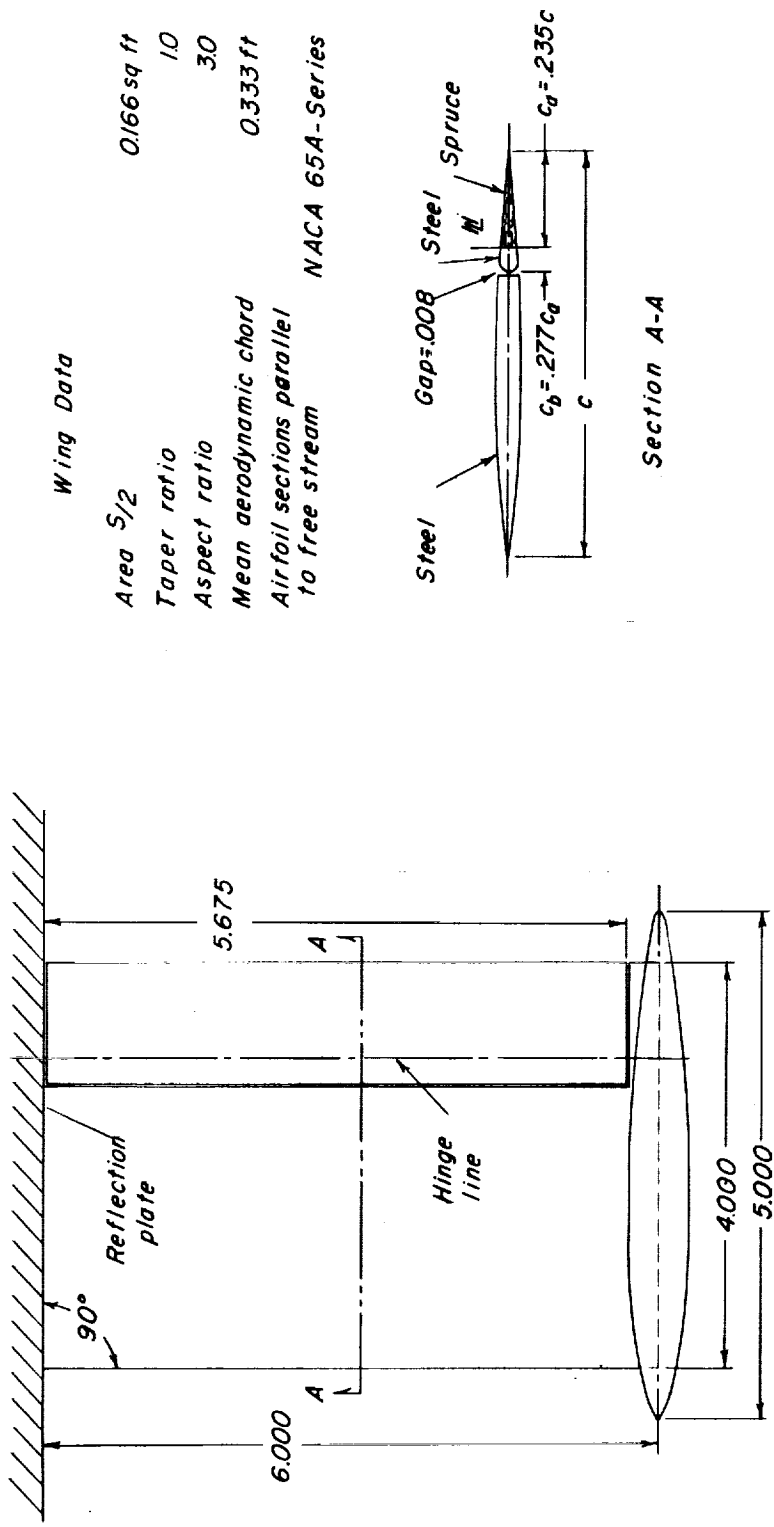
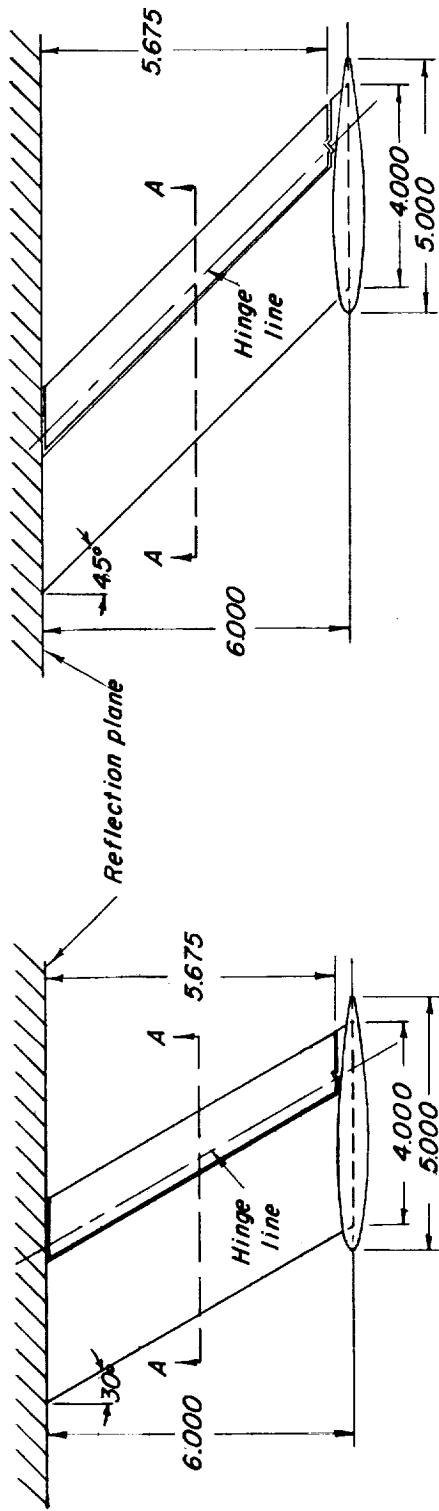


Figure 1.- Schematic drawing of test installation. L-90563.2



(a) Unswept wings.

Figure 2.- General dimensions of models. All dimensions are in inches unless otherwise noted.



30° Swept wing

Wing Data

45° Swept wing

Area, $S/2$	0.166 sqft	Gap = .008	Steel	Steel	h	Spruce	$c_a = .235c$
Taper ratio	1.0	Steel					
Aspect ratio	3.0						
Mean aerodynamic chord	0.333 ft						
Airfoil sections parallel to freestream	NACA 65A006						

Section A-A

(b) Swept wings; $t/c = 0.06$.

Figure 2.- Concluded.

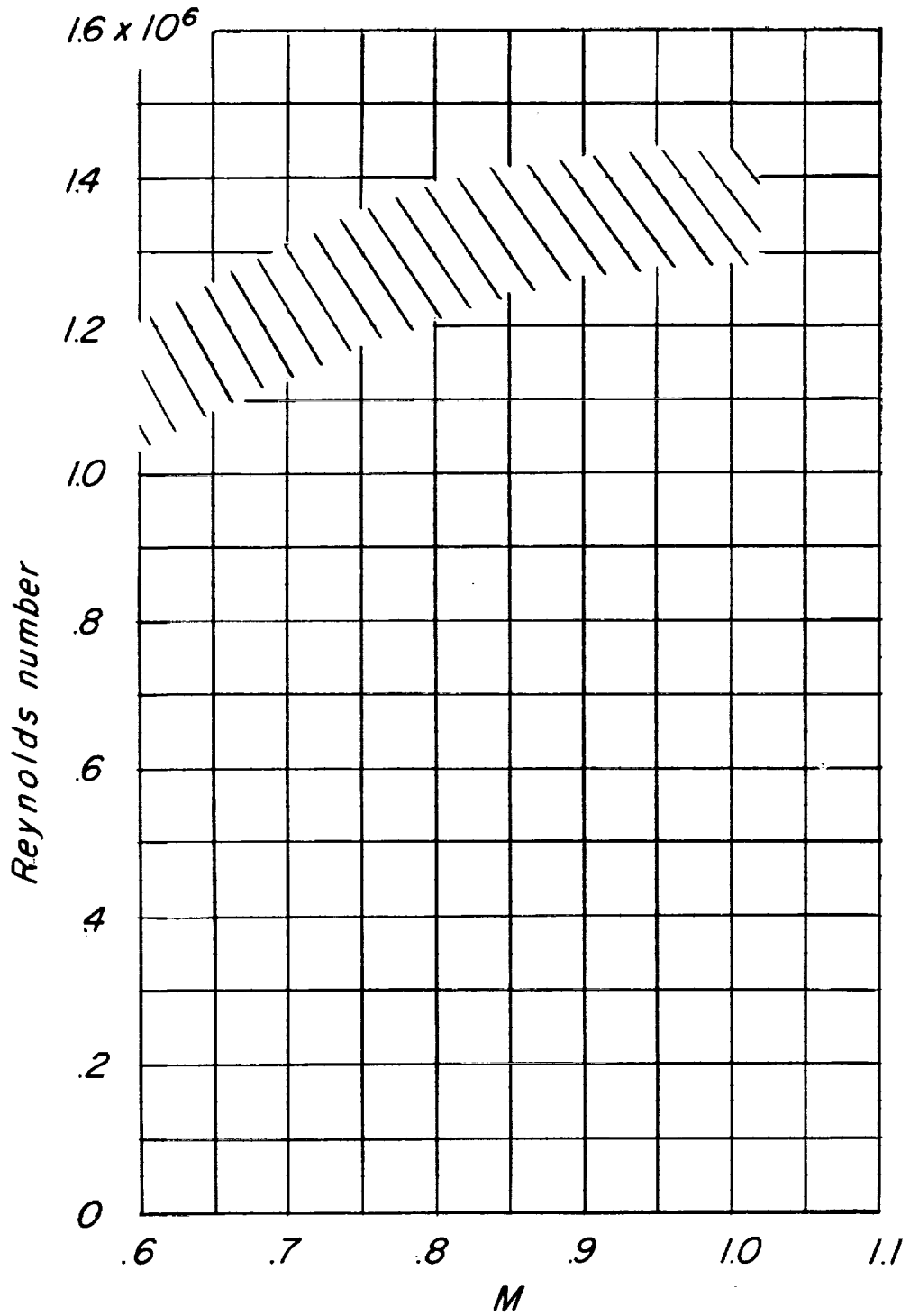
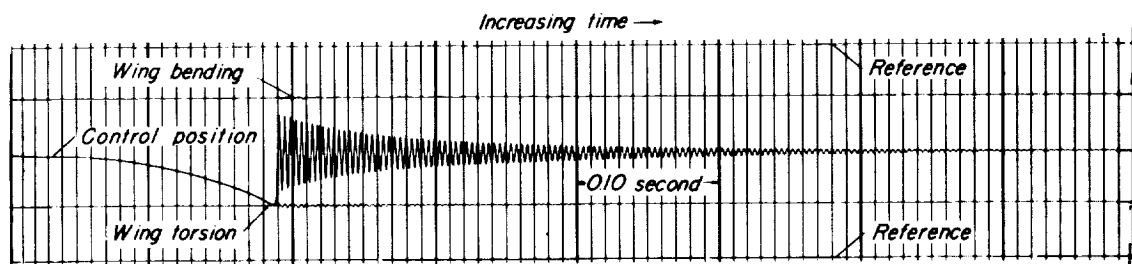
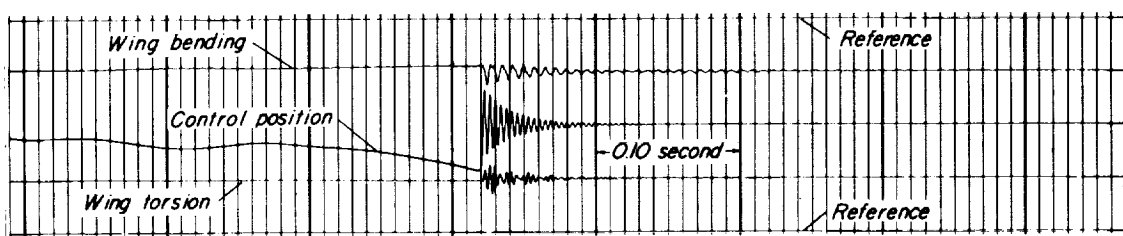


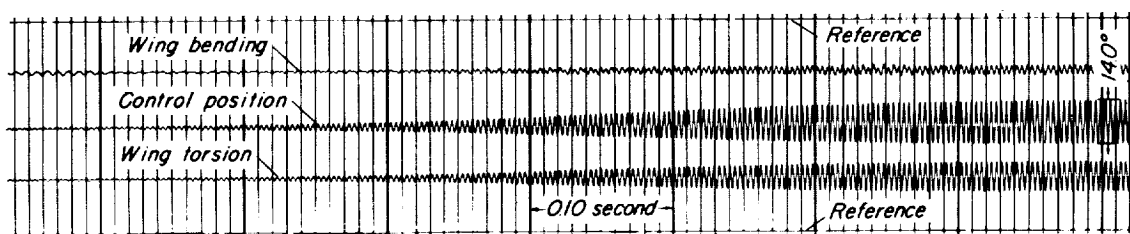
Figure 3.- Variation of Reynolds number with Mach number.



(a) Wind off; control released at $\delta \approx 12^\circ$.

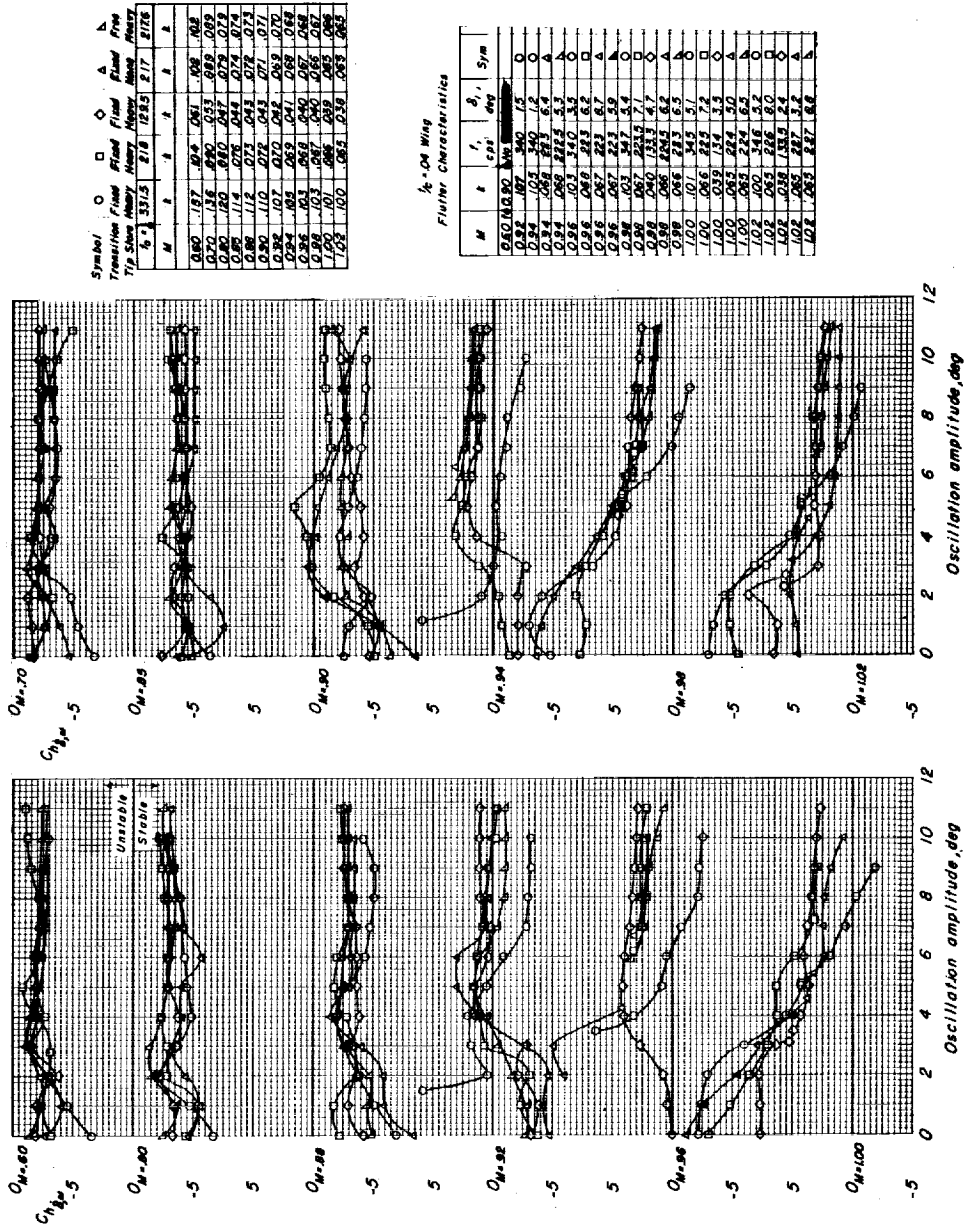


(b) $M = 0.70$; control released at $\delta \approx 12^\circ$.



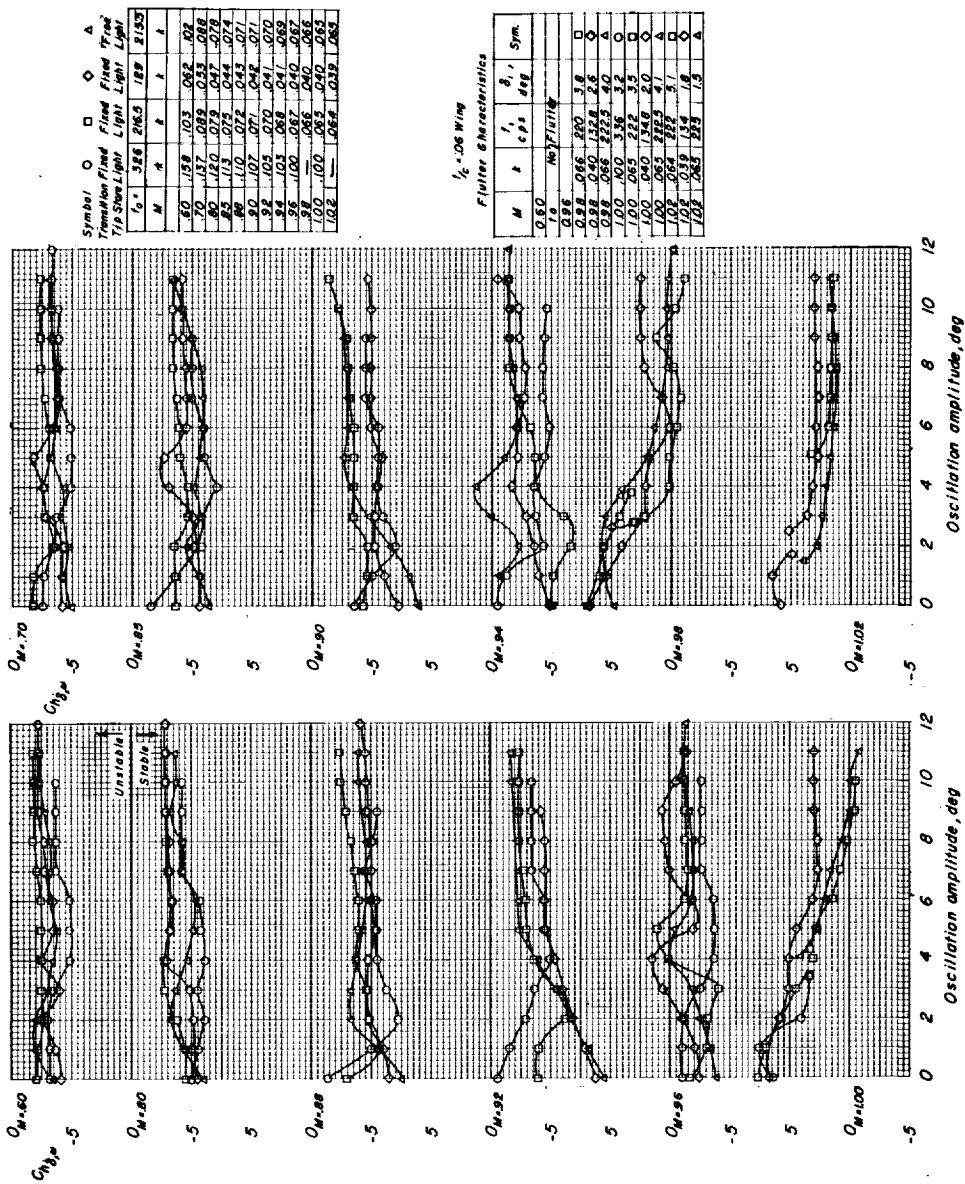
(c) $M = 1.01$; control released at $\delta \approx 0^\circ$.

Figure 4.- Oscillograph records.



(a) Wing with $t/c = 0.04$.

Figure 5.- Variation of damping derivative with oscillation amplitude for various Mach numbers and control frequencies. Unswept wings.



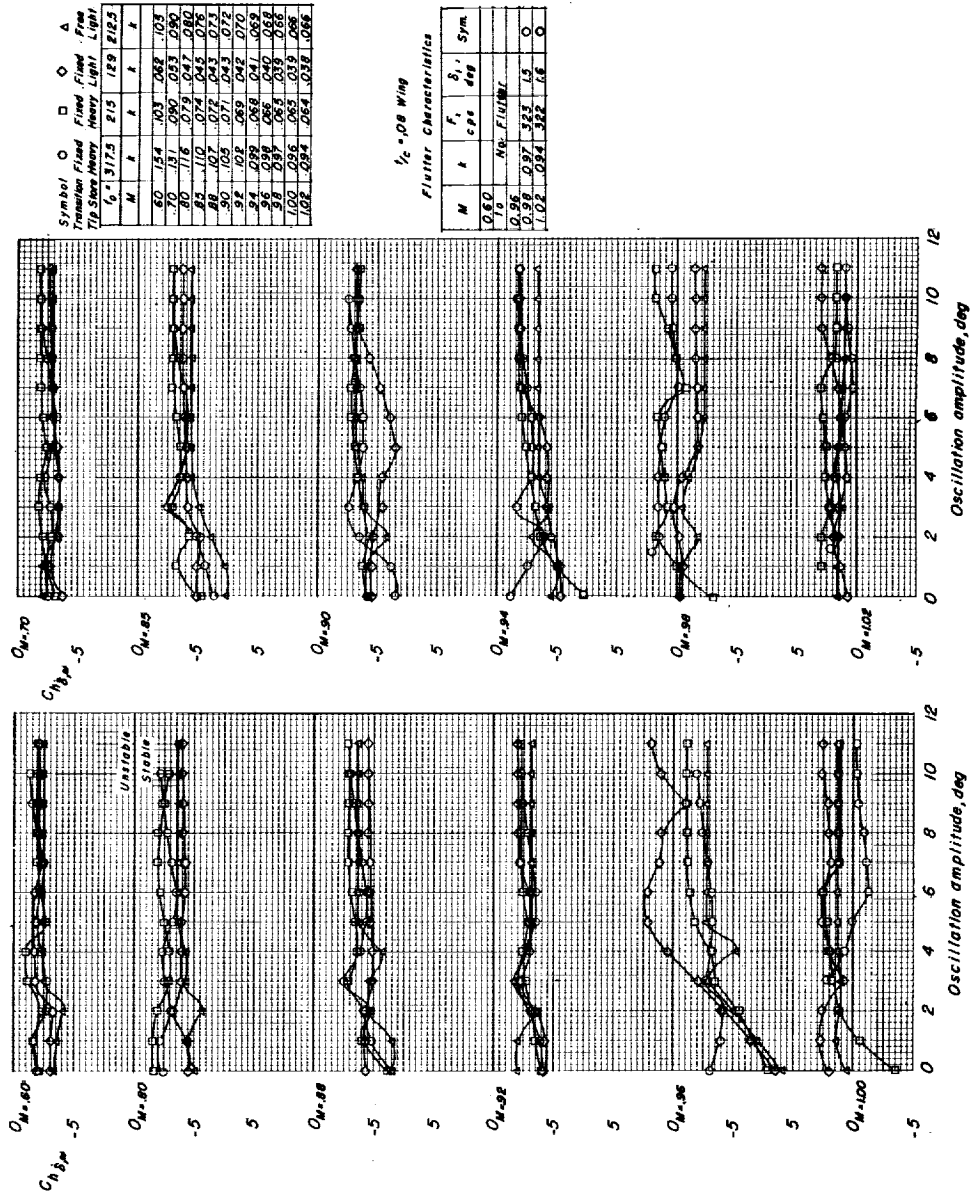
Symbol	Fixed	Fixed	Fixed	Fixed	Fixed
Transmission	Light	Light	Light	Light	Light
α_0	3.66	2.65	1.89	2.152	
M	0.70	0.80	0.90	0.94	0.98
β	0.158	0.103	0.062	0.02	0.02
γ	0.137	0.092	0.053	0.02	0.02
δ	0.120	0.079	0.047	0.02	0.02
ϵ	0.113	0.075	0.044	0.02	0.02
ζ	0.107	0.071	0.042	0.02	0.02
η	0.102	0.070	0.041	0.02	0.02
θ	0.101	0.068	0.041	0.02	0.02
ι	0.100	0.067	0.040	0.02	0.02
κ	0.100	0.066	0.040	0.02	0.02
λ	0.100	0.064	0.039	0.02	0.02

1/4 Scale Wing
Flutter Characteristics

M	β	γ	δ	Sym.
0.60	0.10	0.10	0.10	
0.80	0.066	0.066	0.066	
0.90	0.042	0.042	0.042	
0.94	0.02	0.02	0.02	
0.98	0.02	0.02	0.02	
1.00	0.02	0.02	0.02	
1.02	0.02	0.02	0.02	

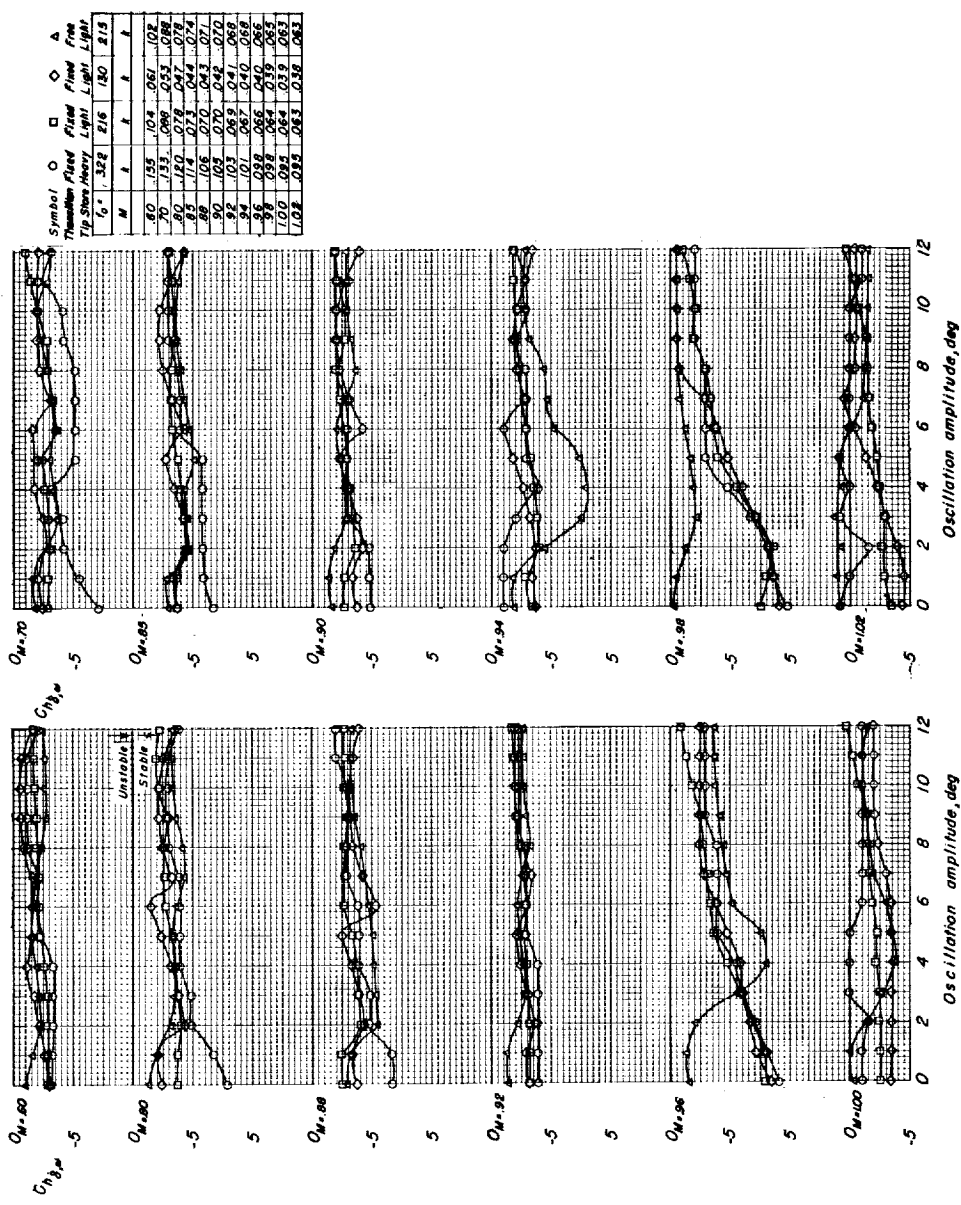
(b) Wing with $t/c = 0.06$.

Figure 5.- Continued.



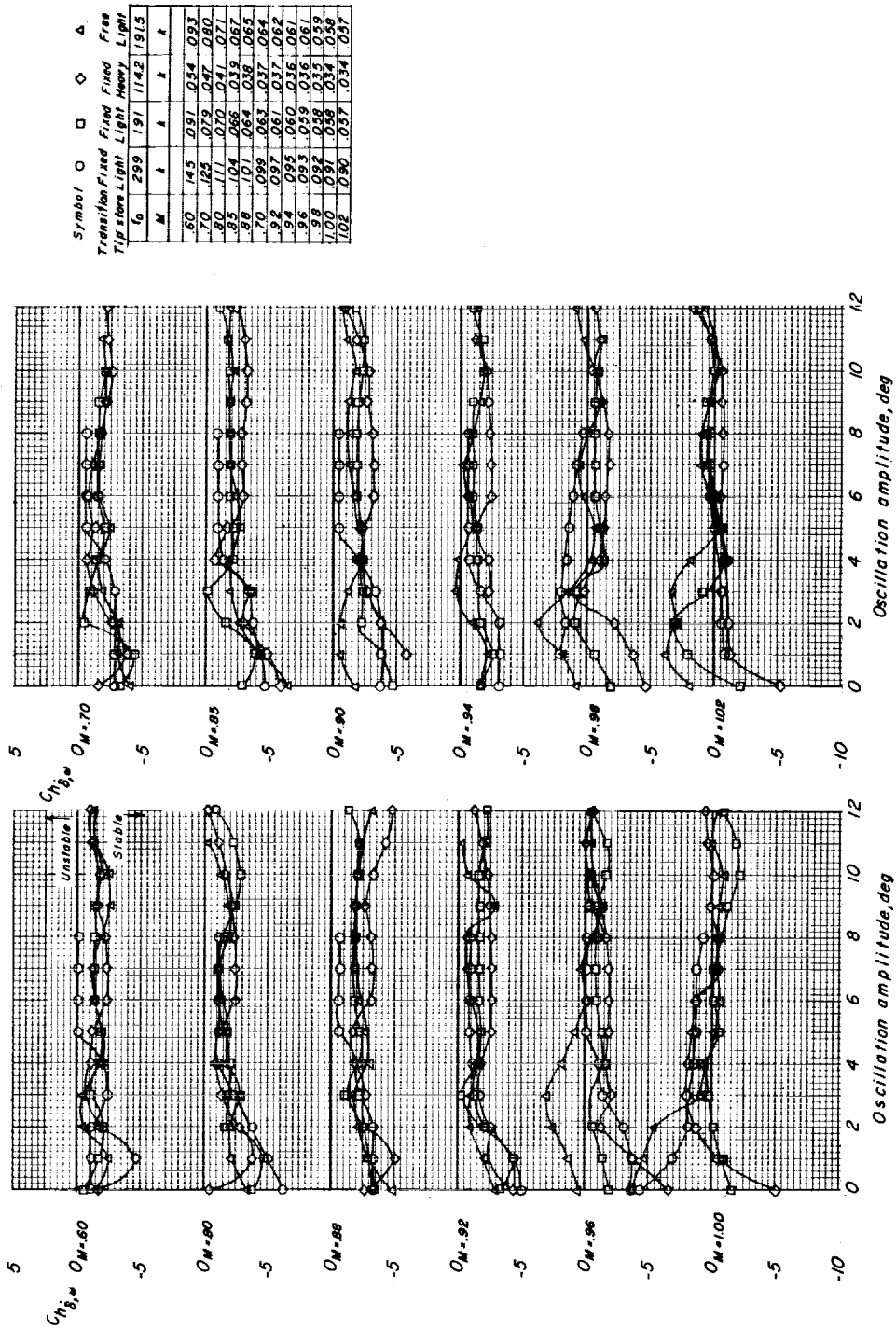
(c) Wing with $t/c = 0.08$.

Figure 5.- Continued.



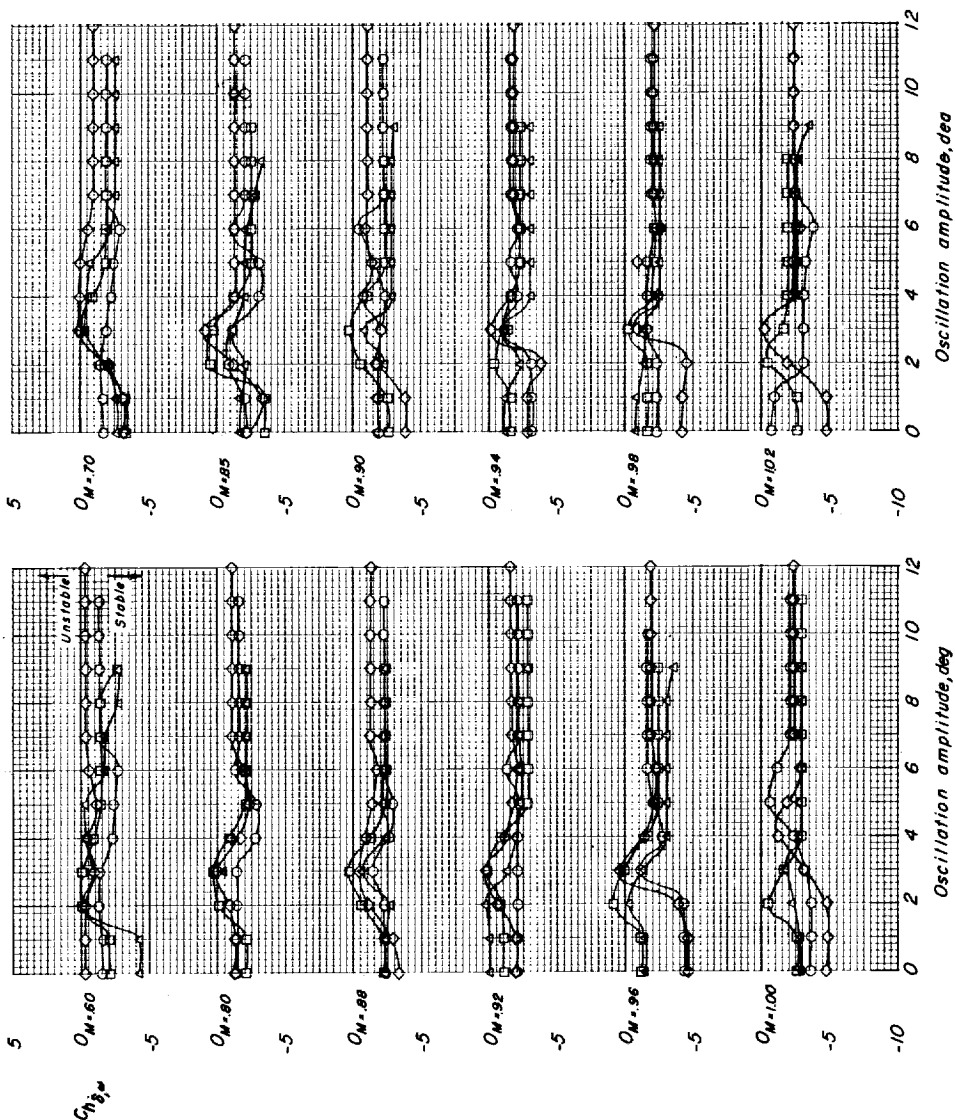
(d) Wing with $t/c = 0.10$.

Figure 5.- Concluded.



(a) 30° swept wing.

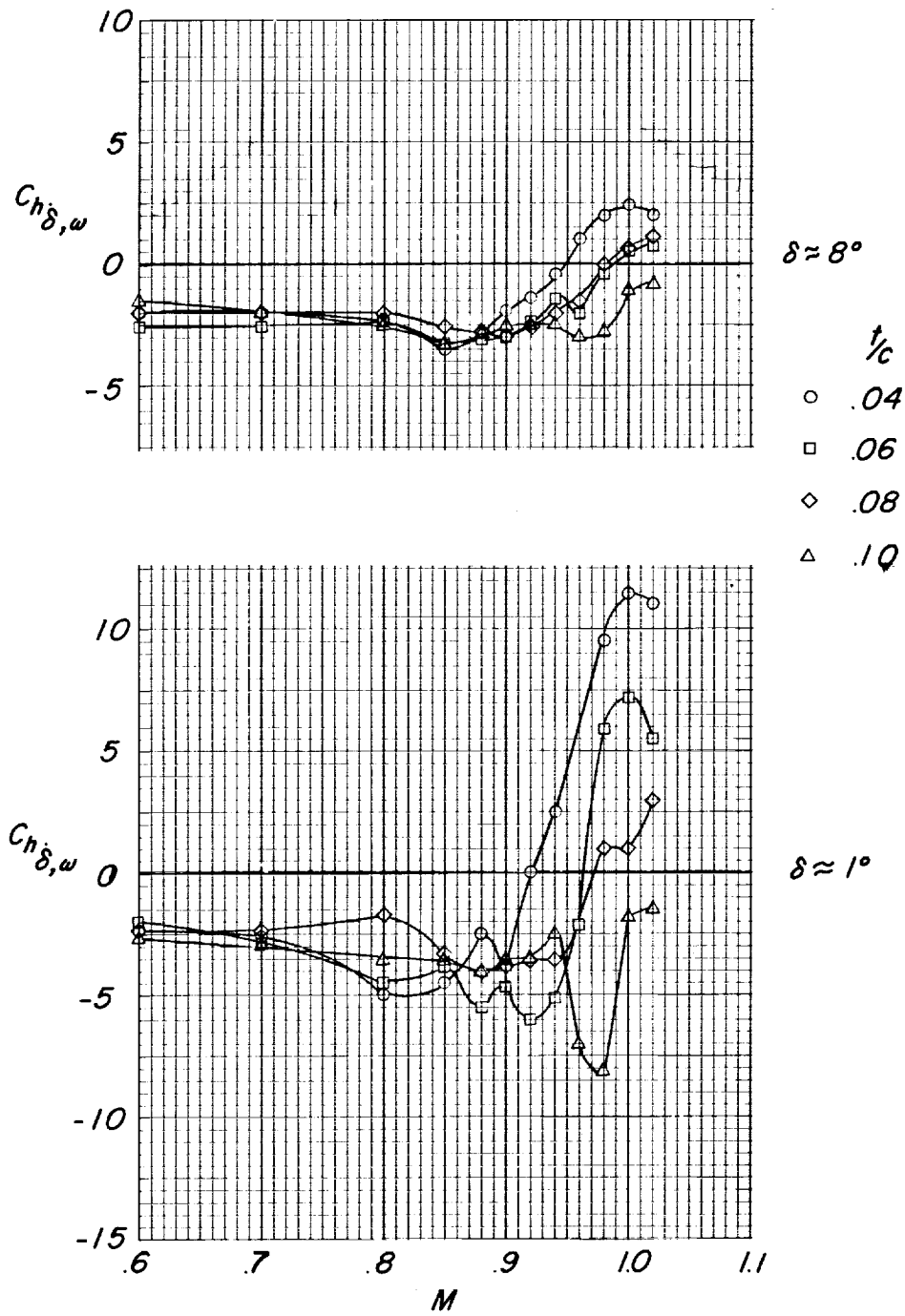
Figure 6.- Variation of damping derivative with oscillation amplitude for various Mach numbers and control frequencies. $t/c = 0.06$.



Symbol	Transition			Fixed			Free		
	Tip slope	Light	Heavy	Light	Heavy	Light	Heavy	Light	
ζ	303	194	116	116	116	116	116	195	
M	ζ	ζ	ζ	ζ	ζ	ζ	ζ	ζ	
60	.142	.084	.054	.055	.093				
70	.124	.080	.048	.048	.081				
80	.110	.071	.042	.042	.071				
85	.104	.067	.039	.039	.067				
88	.101	.065	.038	.038	.065				
90	.099	.064	.037	.037	.064				
92	.097	.062	.037	.037	.062				
94	.095	.061	.036	.036	.060				
96	.093	.059	.035	.035	.058				
98	.091	.058	.034	.034	.056				
100	.088	.056	.034	.034	.056				
102	.088	.057	.034	.034	.057				

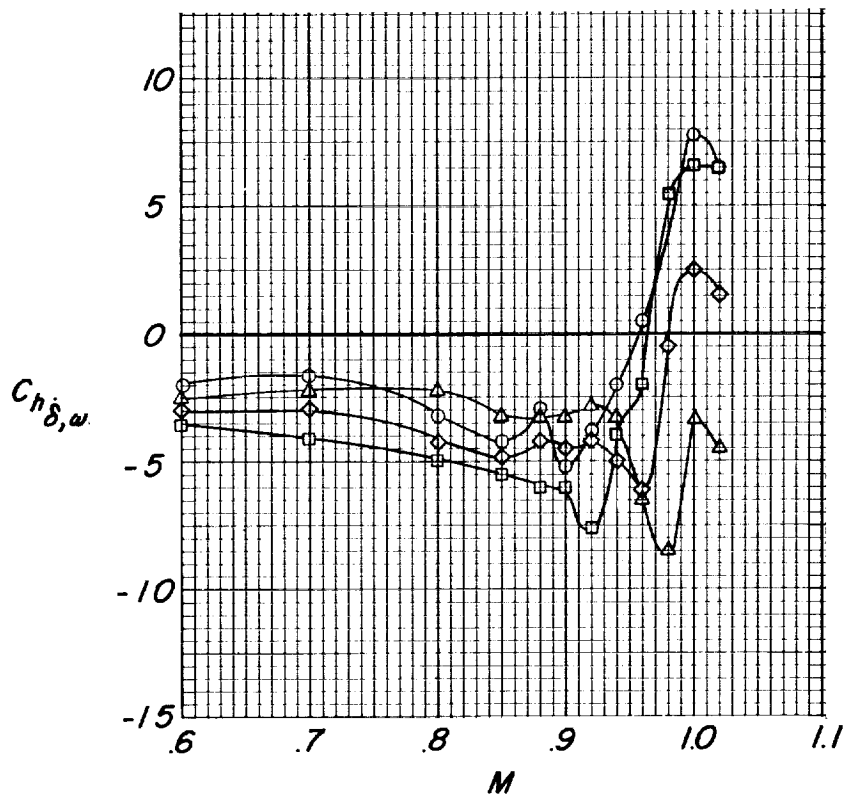
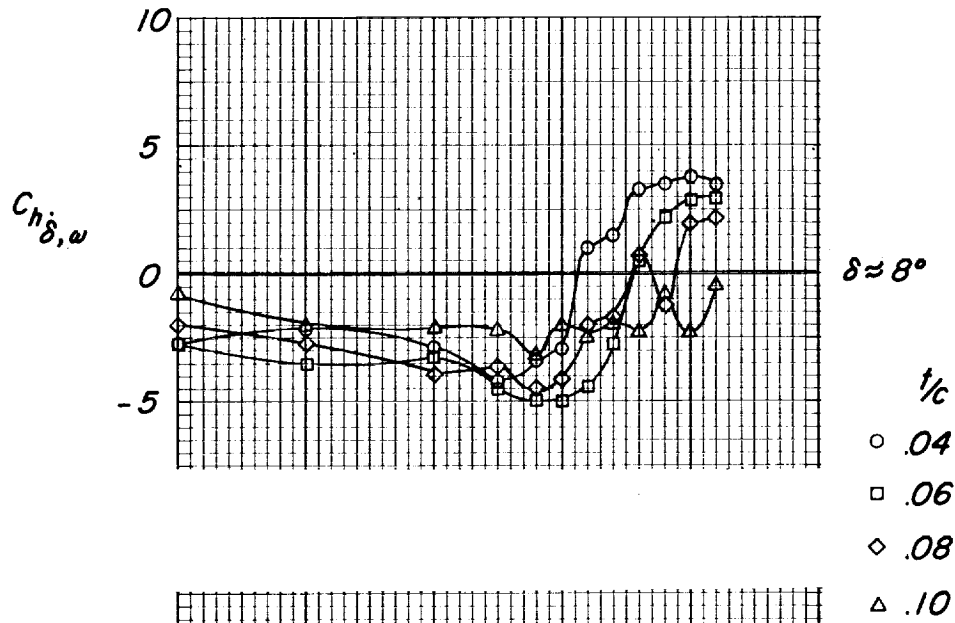
(b) 45° swept wing.

Figure 6.- Concluded.



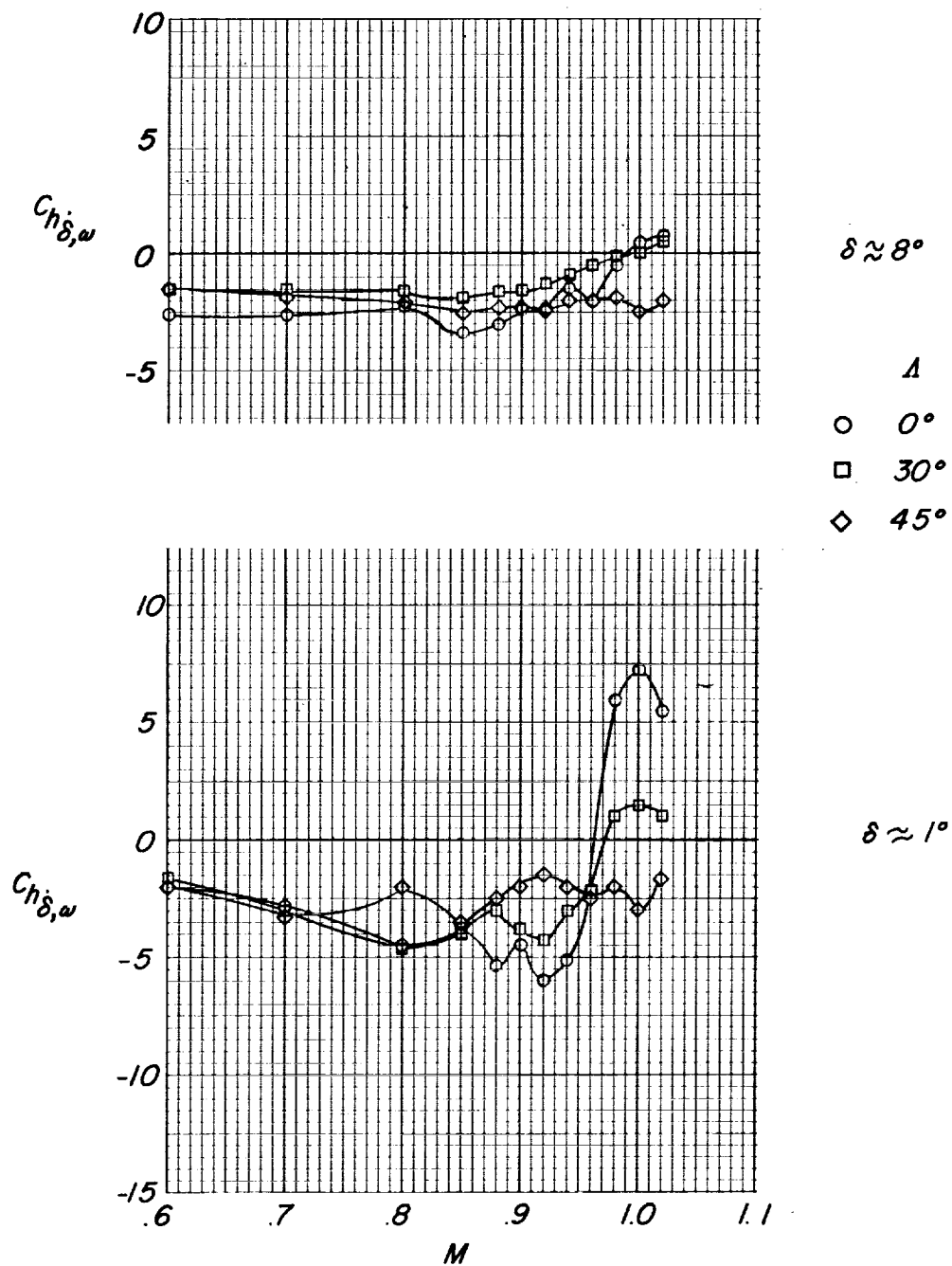
(a) $k \approx 0.08$.

Figure 7.- Effect of wing thickness on the variation of damping derivative with Mach number. Unswept wings.



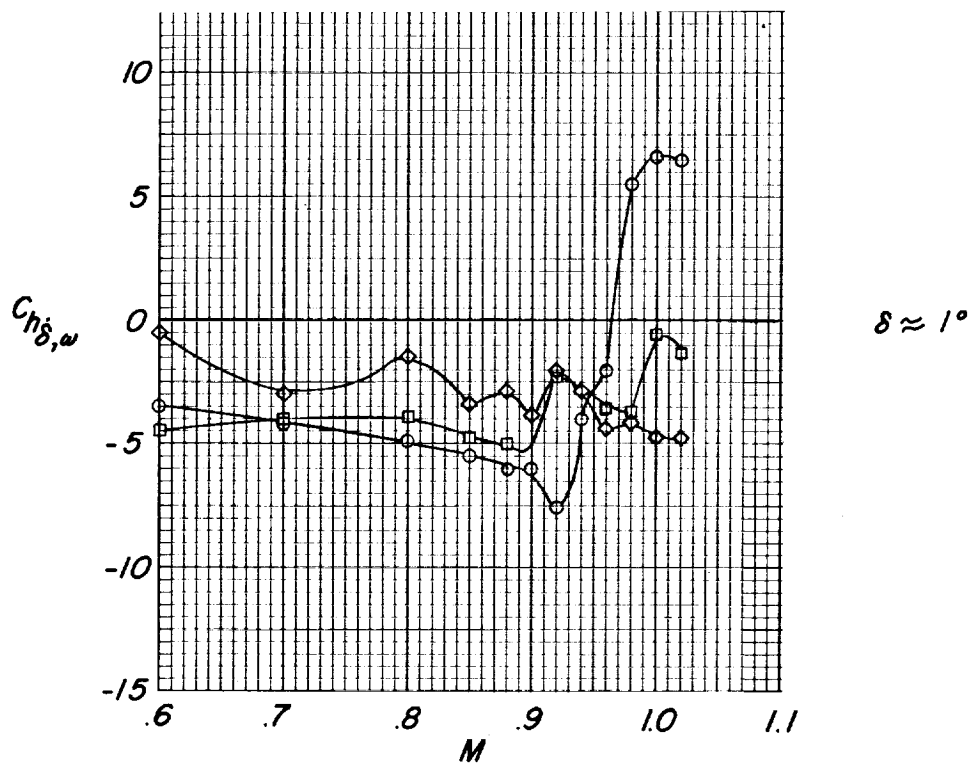
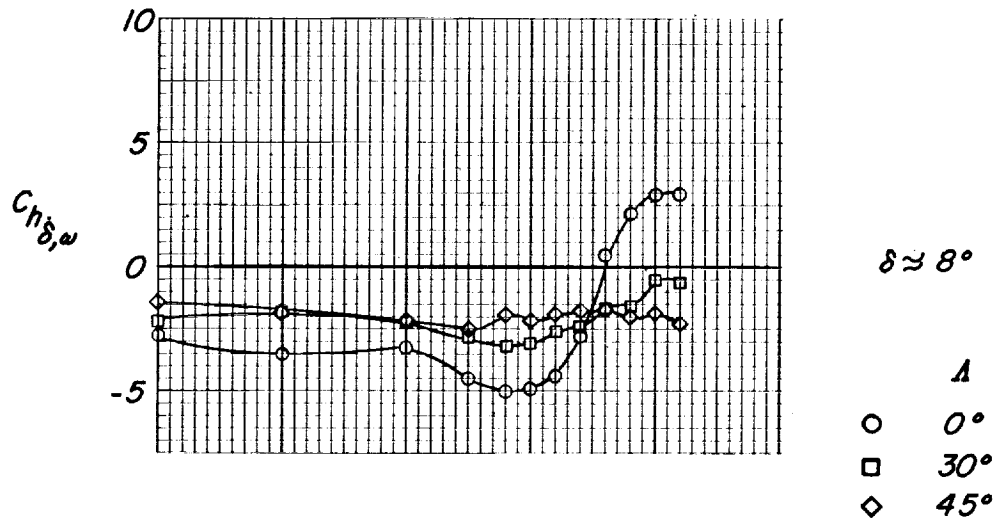
(b) $k \approx 0.04$.

Figure 7.- Concluded.



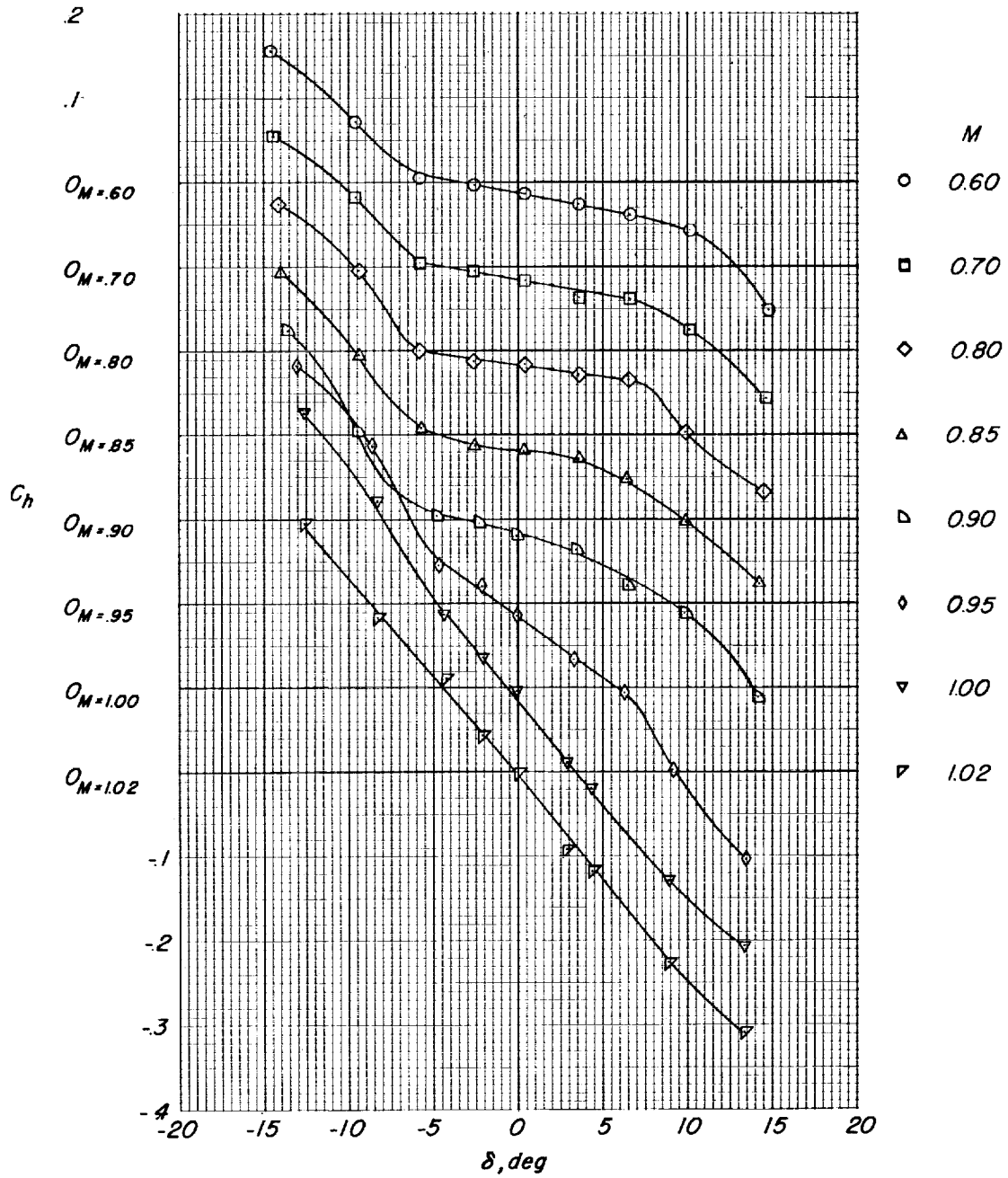
(a) $k \approx 0.08$.

Figure 8.- Effect of wing sweep on the variation of damping derivative with Mach number. $t/c = 0.06$.



(b) $k \approx 0.04$.

Figure 8.- Concluded.



(a) Wing with $t/c = 0.04$.

Figure 9.- Variation of static hinge-moment coefficient with control deflection for various Mach numbers. Unswept wings.

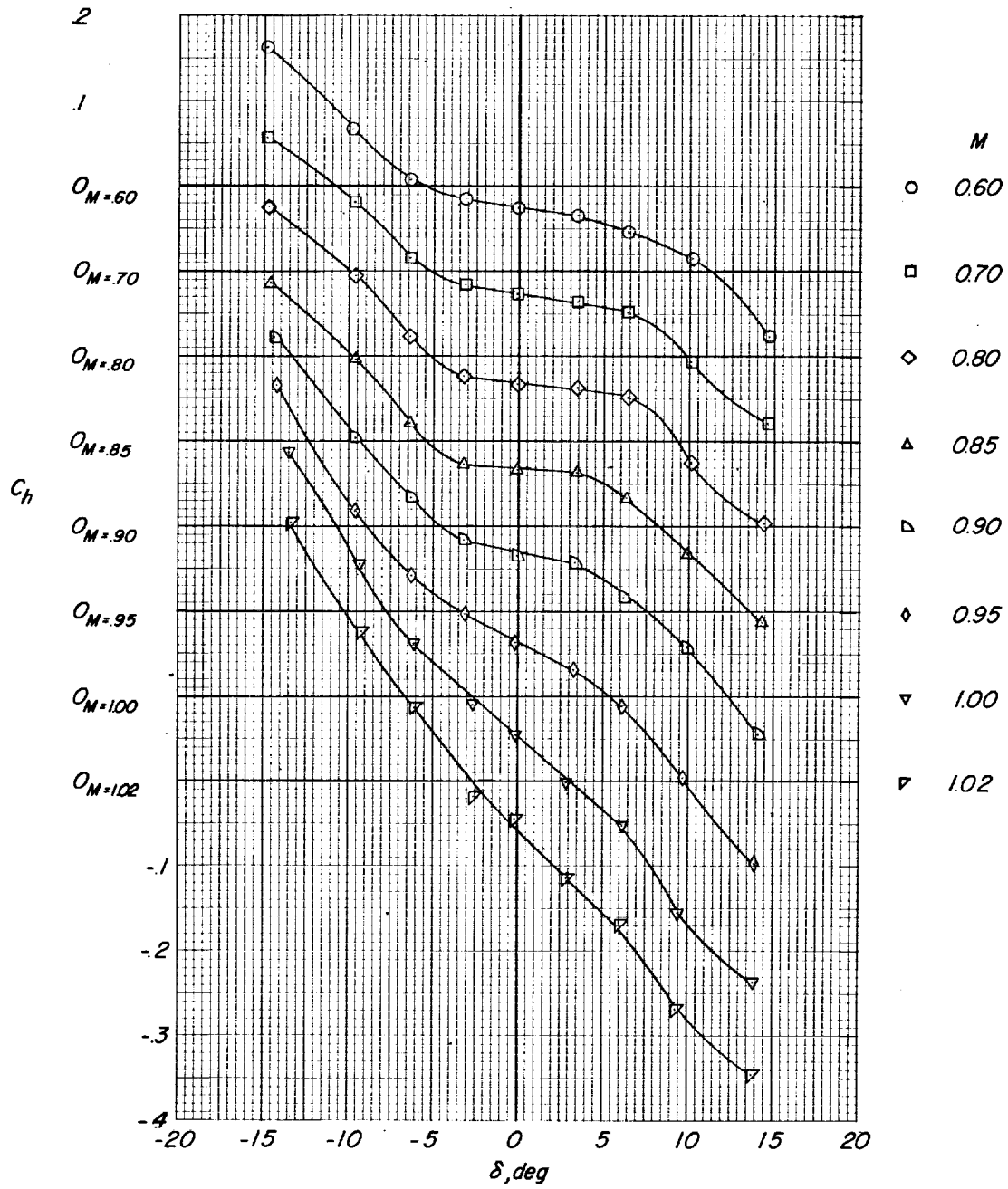
(b) Wing with $t/c = 0.06$.

Figure 9.- Continued.

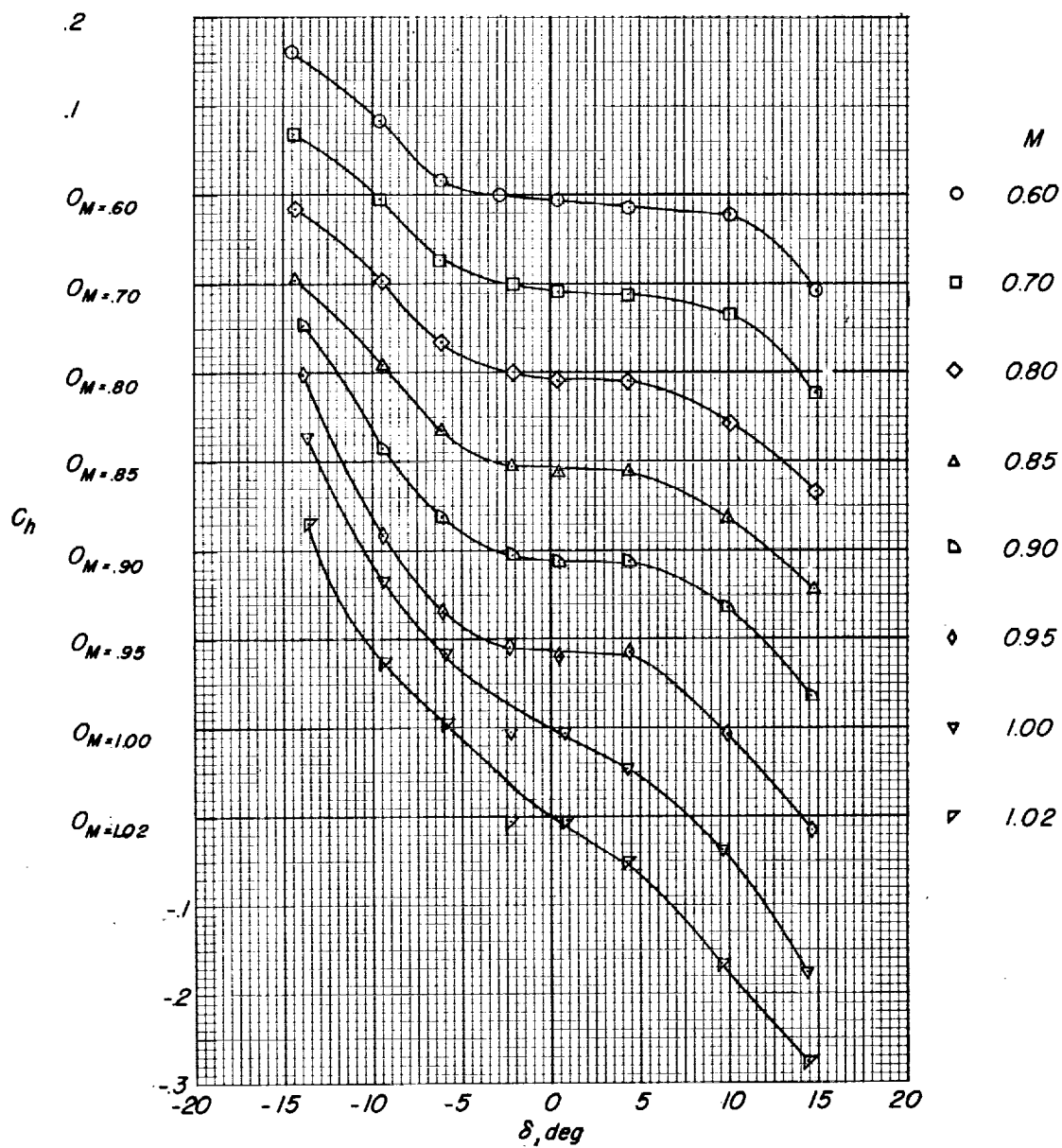
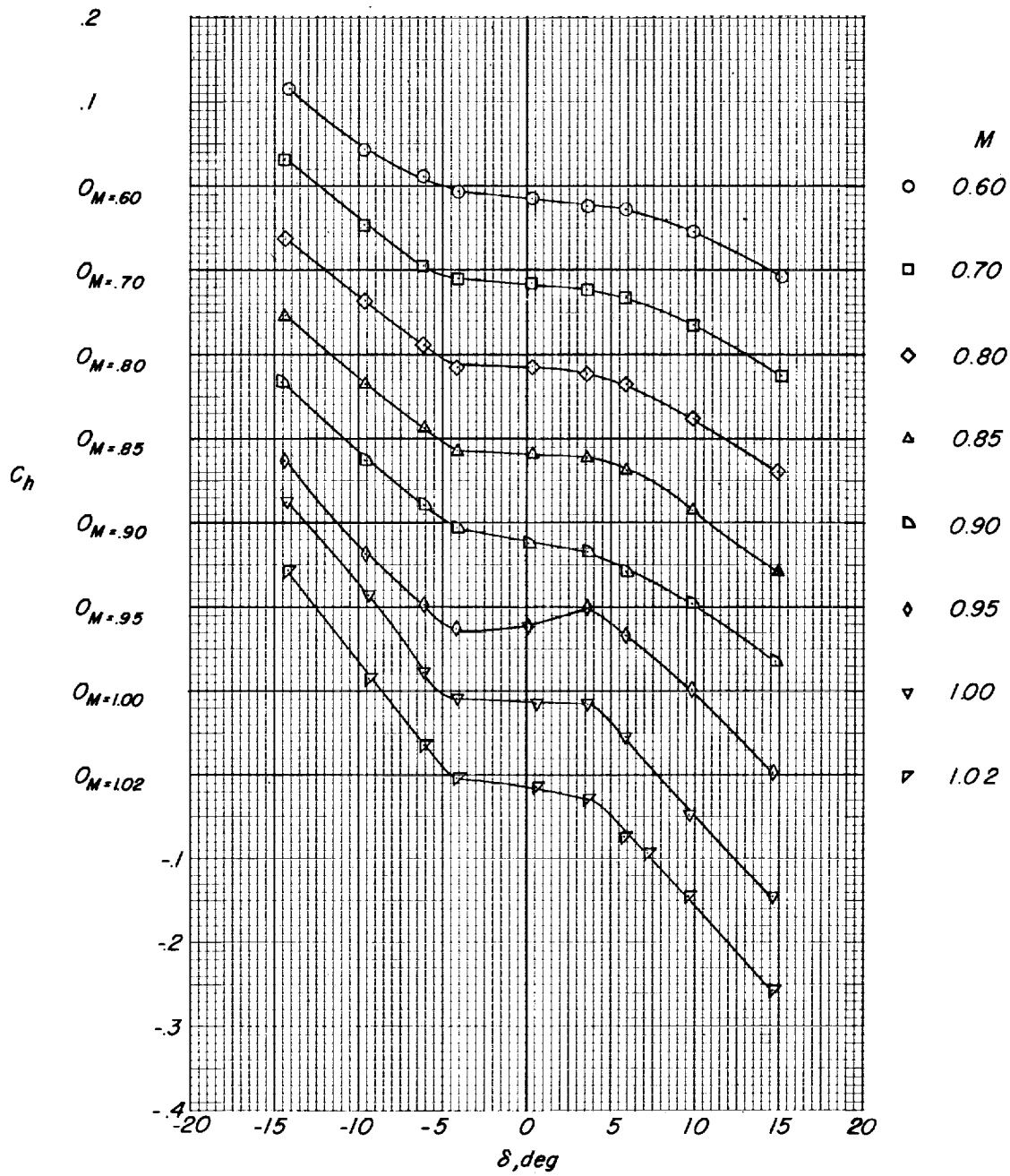
(c) Wing with $t/c = 0.08$.

Figure 9.- Continued.



(d) Wing with $t/c = 0.10$.

Figure 9.- Concluded.

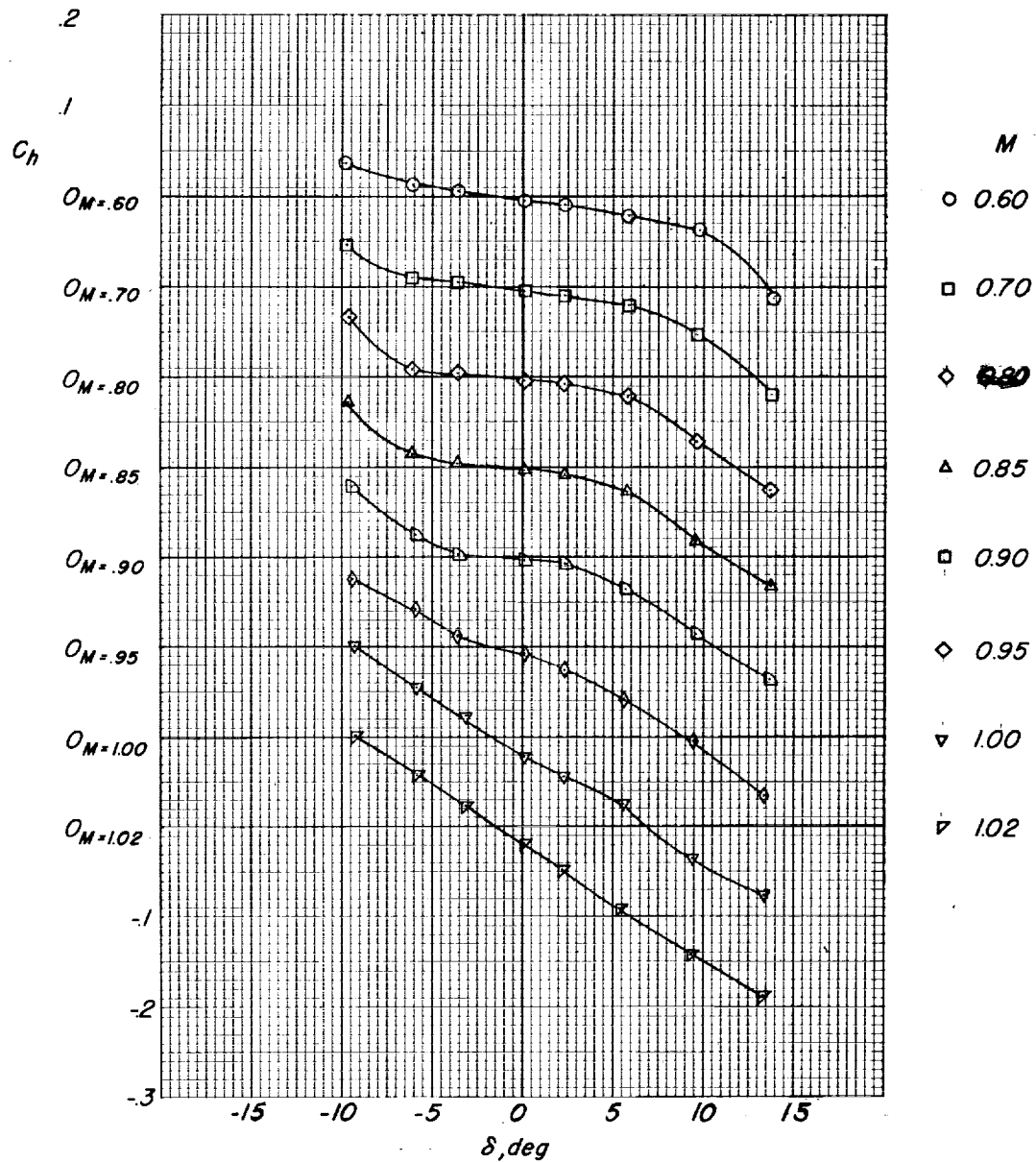
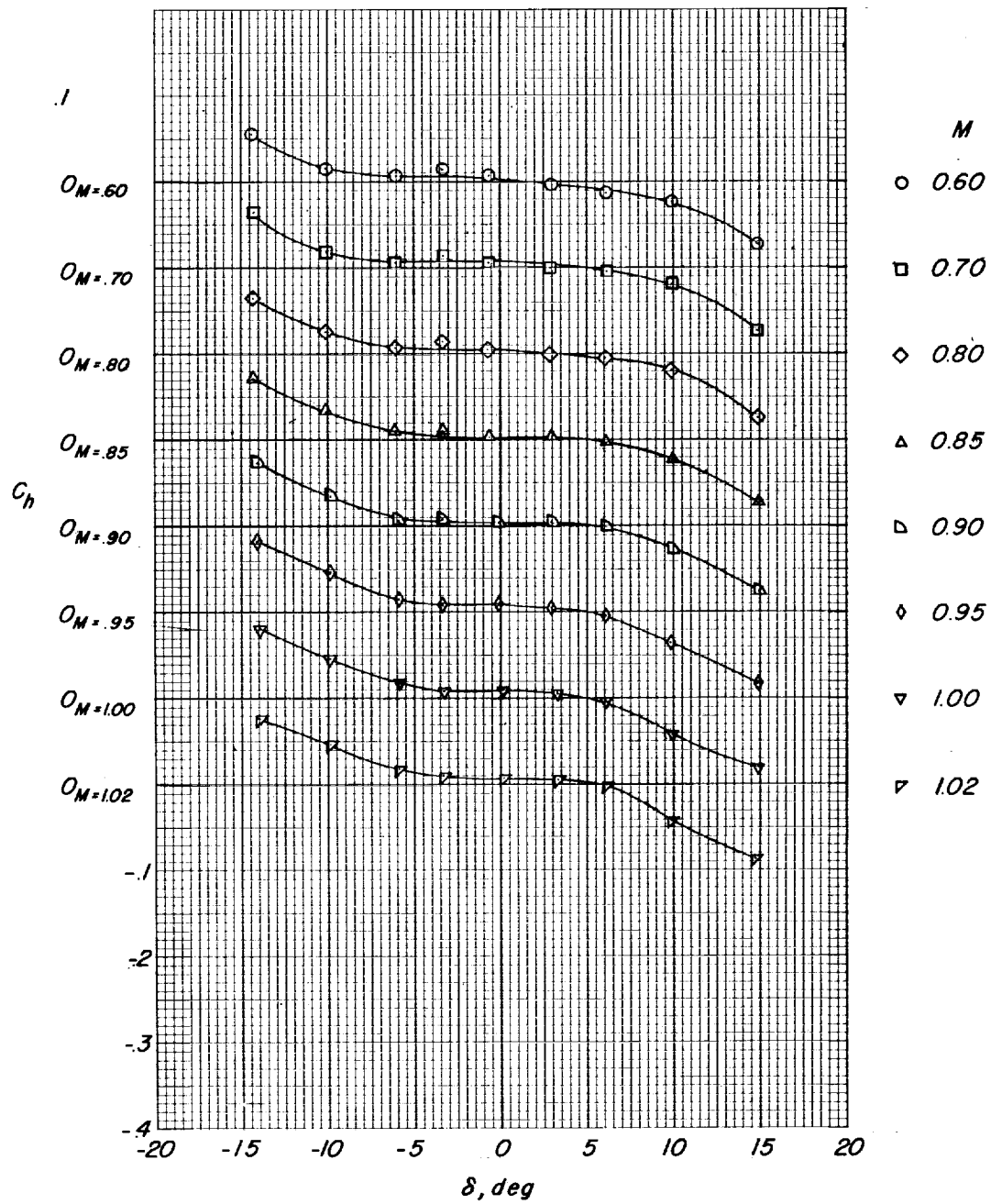
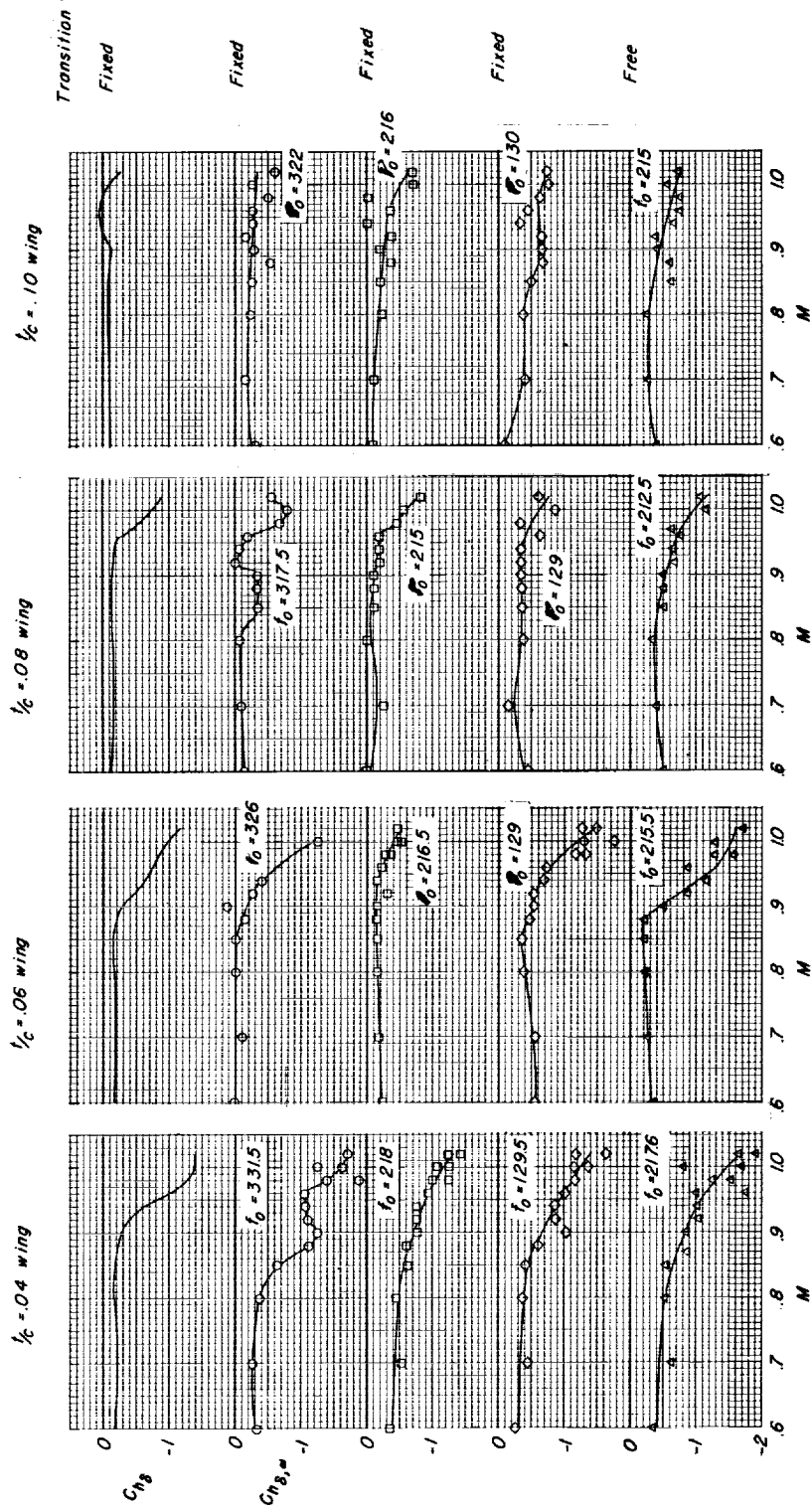
(a) 30° swept wing.

Figure 10.- Variation of static hinge-moment coefficient with control deflection for various Mach numbers. Swept wings; $t/c = 0.06$.



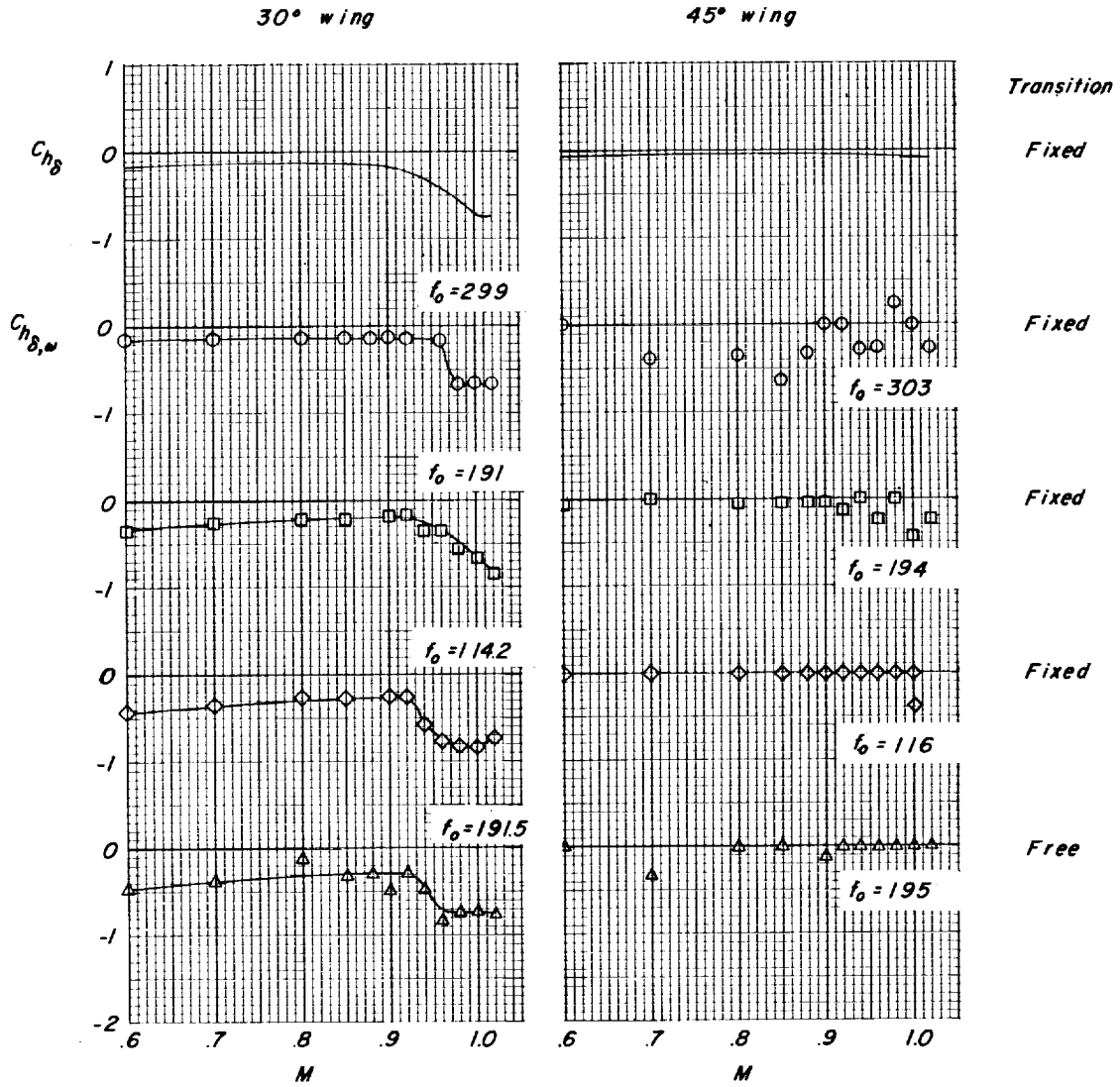
(b) 45° swept wing.

Figure 10.- Concluded.



(a) Unswept wings.

Figure 11.- Variation of Ch_δ and $Ch_{\delta,\omega}$ for the various wings tested.



(b) Swept wings; $t/c = 0.06$.

Figure 11.- Concluded.

